

Geochemical characteristics of submarine rhyolitic pumice from Andaman subduction zone: inferences on magmatism and tectonics of Northeastern Indian Ocean

**Abhishek Saha^{1,2*}, Nessa G. D'Mello^{3,4}, Simontini Sensarma¹, Abhay V. Mudholkar¹,
K.A. Kamesh Raju¹, Bhagyashree Doley^{1,2},**

¹CSIR-National Institute of Oceanography, Dona Paula, Goa 403 004, India

²Academy of Scientific and Innovative Research, Ghaziabad, Uttar Pradesh 201 002, India

³Department of Geology, University of Pune, Pune 411 007, India

⁴Volcanic Risk Solutions, Institute of Agriculture and Environment, Massey University,
Private Bag 11 222, Palmerston North, New Zealand
E-mail: asaha.nio2015@gmail.com; asaha@nio.org

Abstract

This paper reports new geochemical data for submarine volcanic pumice sampled from two volcanoes (SM-1 and SV-1) which are part of the Andaman subduction system. SM-1 volcano is located closer to the Andaman back-arc spreading axis while SV-1 volcano is part of a linear chain of arc volcanoes in the southern Andaman Basin. The pumice are products of phreatomagmatic eruptions and are highly vesicular in nature, however immediately after eruption of these lava froth, sea-water entering into the vesicles made them sink to the sea-floor. A sheet of dull grey to white colored pumice observed on top of the SM-1 volcano indicates a non-explosive eruption referred to as Tangoroan type. Pumice from these two spatially apart volcanoes share uniform physical properties but display minor variations in mineralogical compositions and distinct characteristics of selected major and trace elements. Pumice from SM-1 comprises plagioclase, hornblende, and spinel while those from SV-1 are composed of plagioclase and quartz as main crystalline phases. Geochemically, the pumice samples from SM-1 volcano are classified as medium-K calc-alkaline rhyolites, while those from SV-1 volcano show low-K tholeiitic compositions. Trace and REE compositions for these rhyolitic pumice collectively reflect LILE-LREE enriched, HFSE depleted signatures of subduction zone magmatism and implicate an oceanic arc tectonic affinity. Selective enrichment in LILE and LREE with relative HFSE depletion is attributed to infiltration of fluid-mobile LILE and LREE into the mantle via fluids released from slab-dehydration with retention of fluid-immobile HFSE in the subducted slab. Elevated abundances of LILE/HFSE, LREE/HFSE and LREE/HREE for the medium-K calc-alkaline rhyolitic pumice relative to their low-K tholeiitic counterparts invoke increased fluid-flux into the mantle with progressive maturation of oceanic slab subduction. The precursor magmas parental to the SM-1 and SV-1 volcanic pumice were derived by partial melting of a mantle wedge metasomatized by variable slab-mantle interactions, and influx of slab-dehydrated fluids and sediments. Pronounced REE fractionation trends suggest evolution of resultant melts in a cold, hydrous, oxidizing regime of intraoceanic arc setting that eventually reheated, remelted, remobilized and assimilated lower oceanic arc crust and erupted as rhyolites. The volcanic pumice from Andaman are geochemically and tectonically analogous to those from Mariana arc and Okinawa Trough of Pacific Ocean.

Keywords: Andaman arc-back arc, pumice, rhyolite, oceanic arc, slab-dehydration, fluid-flux

1. Introduction

In the Phanerozoic Earth (~540 Ma to present day), subduction comprises a major component of global plate tectonics and it is the most significant mechanism for recycling of rocks, sediments, water and volatiles from the surface into the mantle that posit profound effect on the geological, geochemical and geophysical evolution of the Earth. Three quarters of the Earth's volcanic activity occurs beneath the sea. Submarine volcanism constitutes an important component of active island arc systems. Arc-back arc magmatism associated with active oceanic subduction systems provide the best window to understand the sinking of oceanic lithosphere into the mantle and the consequent processes such as partial melting, mantle wedge metasomatism and hybridization, dehydration, melting, delamination and recycling of subducted oceanic slab. These processes collectively enhance ocean-crust-mantle interaction, hydrothermal activity, ore mineralization and magmatism of diverse compositional spectra. Felsic magmatism shows marked genetic correlation with subduction related tectonic activities in terms of both ocean-ocean and ocean-continent convergence and their emplacements provide viable evidence for distinct episodes of oceanic and continental crust generation (Stern, 1991; Leat and Larter, 2003). Arc-back arc magmatism in active intraoceanic convergent plate margin setting is distinctly characterized by bimodal mafic-felsic volcanism and tholeiitic to calc-alkaline BADR (basalt-andesite-dacite-rhyolite) varieties that play key role in generation, evolution and accretion of juvenile oceanic crust. Partial melting of sub-arc mantle wedge and altered, metamorphosed subducted oceanic lithosphere are the two principal proponents for arc magmatism with variable extents of slab-mantle-crust interaction spanning over incipient to matured stages of subduction (Saha *et al.*, 2018a). Felsic magmatism is predominantly a product of subcrustal and intracrustal melting associated with magmatic arcs at convergent plate margins (Brown, 2009). In oceanic and continental arc systems, the overriding plate (oceanic or continental), the subducted oceanic slab and the mantle wedge contribute to the generation of felsic magmas and crust formation (Maruyama *et al.*, 2009). The geochemical trends in young arc volcanic rocks are attributed to contributions from slab components as well as to melting, assimilation, storage and homogenization (MASH) processes in the arc crust (Stern, 1991; Goss *et al.*, 2013).

The Andaman arc-back arc system in the north-eastern Indian Ocean exemplifies an active intraoceanic convergent margin with minimal effect of continental crust assimilation and a potential site for elemental fractionation between subducted oceanic crust, adjacent mantle wedge and overriding oceanic plate. Arc magmatism is characterized by calc-alkaline volcanism with andesites as main rock types. The extreme fractionation product of the calc-alkaline volcanism is dacite/rhyolite which occurs in the form of pumice and is considered as volcanic froth. There are many

reports of ophiolites and subduction zone volcanism from various islands of the Andaman Sea (Haldar *et al.*, 1992; Pal *et al.*, 2003; 2007; Haldar and Luhr, 2003; Ray *et al.*, 2012; Sheth *et al.*, 2009; 2010; 2011, Sheth, 2014, Saha *et al.*, 2010; 2018b and references therein) especially the recently erupted Barren Island volcano. However, there are almost no studies on the submarine arc volcanics from the Andaman subduction zone. In this paper a comprehensive physical, petrological and geochemical study of pumice dredged from two far apart submarine volcanoes of the Andaman subduction zone is presented. The observations and interpretations have been used to discuss the styles of eruption, mantle melting conditions, crust-mantle interactions, petrogenetic processes, and tectonic implications to address the origin and evolution of felsic magmas in an active intraoceanic arc- back arc regime.

2. GEOLOGICAL SETTING

The oblique under-thrusting of the Indo-Australian Plate under the Eurasian Plate due to the northward movement of the Indian Plate has resulted in the formation of a subduction zone in the north eastern portion of the Indian Ocean. The subduction zone is marked by the presence of the trench- arc – back arc system. Andaman - Java - Sumatra trench and Andaman subduction system are part of this tectonic setup. The Andaman Basin (~8,00,000 sq. km area), situated between 6°N and 14°N, and 91°E and 94°E, extends for 1200 km from Myanmar in the north to Sumatra in the south and 650 km wide with the Malay Peninsula in the east and the Andaman and Nicobar Islands in the west (Rodolfo, 1969; Roy, 1992) (Fig. 1A). In a regional tectonic setup, the Andaman Basin lies along the Indian and Eurasian plate boundary which extends from the Sunda Arc and trench off Java and Sumatra, along the west side of the Andaman- Nicobar Ridge and northward through the Indo-Burmese Ranges (Curry *et al.*, 2005) (Fig. 1A). Bathymetry of the Andaman Sea reveals an average depth of ~1000 m with the northern region being shallow (~600 m) due to continuous sedimentation from the Irrawaddy River draining Myanmar region. Less than 5% of the Andaman Sea has more than 3000 m deep seafloor comprising the submarine valley system with depths of ~4000m (Rodolfo, 1969). Important physiographic features of the Andaman Basin include the Central Andaman Trough, Sewell Seamount in north and Alcock Seamount to the south of the spreading axis (Rao *et al.*, 1996) (Fig. 1A). Andaman Sea is an active back arc extensional basin lying behind the Sunda subduction zone (Kamesh Raju *et al.*, 2004; Curry, 2005) and also identified as a pull-apart basin or leaky transform fault basin that is typical of highly oblique convergence and/ or ridge trench collision (Lodolo *et al.*, 2013). The Indo-Australian plate subducts beneath the SE Asian plate with variations in terms of speed and direction which has resulted in the oblique convergence in the Andaman-Nicobar sector (Kamesh Raju *et al.*, 2004, Subrahmanyam *et al.*, 2008). Seismic activity

with earthquake centers located along the Sunda arc, extending from the eastern Himalayan syntaxis to the Banda arc (Kamesh Raju, 2005) is prominent in the northern part of Andaman arc-back-arc system. The presence of an active volcanic arc is represented by Barren and Narcondam volcanoes with recent volcanic eruptions on Barren Island. Kamesh Raju *et al.* (2012) reported dacites and rhyolites from a volcano situated exactly in the central part of an earthquake swarm.

3. PHYSICAL PROPERTIES OF PUMICE

The rocks are identified as pumice because of their extremely low density, high vesicularity and volcanic mode of formation (Whitham and Sparks, 1986). Physically the rocks are relatively dense and cannot be broken easily, however they float in water.

Physical properties like, specific gravity, dry density, porosity, saturated density of representative pumice samples from SM-1 and SV-1 volcanoes were determined (Table 1). These measurements were made using the representative cubes or small blocks of pumice samples from SM-1 and SV-1, taking into account the maximum variation in vesicle morphology, vesicle density and apparent density within the rock. Physical properties data (Table 1), indicate that the pumice from SM-1 has low vesicularity/ porosity with high specific gravity (2.28) and high density (0.813) as compared to pumice from SV-1 with high vesicularity with low specific gravity (1.84) and low density (0.407). These pumice blocks were also subjected to settling velocity experiment in fresh water and it was observed that SM-1 pumice, having high density, almost immediately sank as compared to SV-1 pumice which took long time; around \geq two weeks to sink. This suggests that high density is not the sole important property for sinking but vesicles also need to be interconnected, due to which water seeps easily throughout the rock and SM-1 pumice sank faster, while porosity of SV-1 pumice is high but the vesicles being not connected, took longer time to sink. It might be due to the type of volcanic eruption that also contributed to the sinking of pumice. The specific gravity of SM-1 pumice is approximately 1.3 times the value of SV-1. Data (Table 1) reveals relatively higher dry density for the SM-1 pumice as compared to SV-1. The porosity values for pumice from both submarine volcanoes show high porosity attributed to the presence of vesicles.

Pumice from SM-1 and SV-1 volcanoes are deep-sea pumice as sampling locations for SM-1 is ~1600m while for SV-1 it is ~1650m which is an important factor that affects the vesicularity (Allen *et al.*, 2010) and other physical properties. The porosity of SV-1 is much higher than SM-1. It seems that the pumice from both volcanoes must have sunk after the phreatic eruption after getting saturated with water which can be called as sinkers (Fiske *et al.*, 2001). Identifying the rocks under

study as pumice suggests a highly vesicular rock and this is reflected in the high porosity for both sets of pumice from SM-1 and SV-1.

4. SAMPLING AND ANALYTICAL TECHNIQUES

Andaman arc- back arc region has been surveyed using different ships like ORV Sagar Kanya, RV Sagar Shukti, MV AA Sidorenko, RV Sonne, etc. During these surveys various geomorphic features including volcanic seamounts were mapped by multibeam system and sampled using dredges. These geomorphic features have been identified and correlated with the regional tectonic setting of the Andaman back arc basin (Kamesh Raju *et al.*, 2004).

A large symmetrical and conical shaped seamount identified as SM-1 (Kamesh Raju *et al.*, 2004), is located in the northern part of volcanic arc (north of the back-arc spreading axis) in the Andaman Sea where it meets West Andaman fault. SM-1 is positioned at 10° 33.646' N and 93° 52.149' E and rises from a depth of 3200m to ~1600m below MSL. The seamount has a typical conical shape with a single high that is centrally located with respect to the circular base of the seamount. The flanks/ slopes of the seamount are jagged/ rough, may be due to the slumping during past volcanic episodes. The SW slope of SM-1 is much steeper than the NE flank of the seamount; characterized by the closely spaced contour lines. SM-1 was dredged and large quantities of fresh unaltered highly vesicular pumice was recovered. (Fig. 1B). During one of the surveys SM-1 volcano was surveyed by Television grab (TV grab) and the observations showed a dull white to grey colored pumice on top. SM-1 volcano does not exhibit any volcanic crater or orifice for eruption of lava.

Another seamount identified as SV-1, is part of a linear chain of volcanoes that form a volcanic arc within the Andaman back-arc basin (Kamesh Raju *et al.*, 2012). SV-1 is located at 07° 26.745' N and 94° 20.645' E and rises from comparatively shallow depth of ~2200m to ~1650m i.e. it is only about 550 m in height. SV-1 has 4 prominent mounds, each at a common depth of ~1650 m. The volcano is irregular in shape and the base can best be described as oval surrounded by smaller volcanic cones at a minimum depth of ~2100 m. The volcano shows steep slopes on all sides except the NE slope having a gentler gradient. Pumice was recovered from this seamount top by dredging. (Fig.1C).

Pumice from SM-1 and SV-1 were mega- and macroscopically observed. Based on nature, density and size and shape of the vesicles, pumice were sub-sampled. Consequently, 9 types of pumice were identified from SM-1 while 10 pumice types were identified from SV-1. These samples were thoroughly cleaned using distilled water in an ultra-sonic bath to remove sediments and salt entrenched during exposure to seawater conditions (Nicholson *et al.*, 2004). Thin sections of pumice

were prepared for mineralogical and vesicle morphology as well for modal analyses. For the determination of physical properties like specific gravity, density, porosity, dry density, etc. small cubes of pumice were prepared from large pumice blocks. Pumice pieces were washed using ultrasonic bath and dried overnight and finely powdered. These finely ground sample (0.5gm) was thoroughly mixed with Merck's Spectromelt[®] A12 flux and borate beads were prepared with Minifuse2 induction furnace for major element oxide content analyzes with PANalytical's Axios WD-XRF.

All selected pumice from SM-1 and SV-1 were analyzed for their major oxides, trace and rare earth elements using XRF and ICP-MS respectively at CSIR-National Institute of Oceanography. Trace and rare earth element concentrations were determined by digesting sample powders (50 mg) with 10 ml of NAM (Normal Acid Mixture, NAM= HF: HNO₃:HClO₄ in the ratio of 7:3:1). Later the solid residue was dissolved in a 4 ml of 1:1 HNO₃ to prepare the clear solution to which 1ml of 1ppm Rh solution was added as a spike and this solution was diluted to 100 ml with MilliQ water for the ICP-MS (Thermo[®] X Series) analysis. Japanese rock standards namely, JR-1 (Rhyolite), JR-3 (Rhyolite) and JA-1 (Andesite), were used as standards to monitor precision and accuracy of the data for both XRF and ICP-MS analyses. Based on these data, accuracy for major element oxides is \pm 3-4% while for the trace element data it is \pm 8%. Major, trace and rare element concentrations for the analyzed pumice samples are listed in Table 2.

5. PETROGRAPHY

5.1 Megascopeic Characters

Macroscopically pumice from both volcanoes show minor variation in color and vesicularity. However, another important observation is that the SM-1 pumice shows presence of small dark colored crystal clots within the glassy matrix, while no mineral or mineral clots are seen in SV-1 pumice. Pumice from SM-1 are off-white in color with black encrustation on localized scale. SV-1 pumice are off-white to grey in color and locally stained yellow with minor signs of charring.

5.2 Microscopic Characters

SM-1

SM-1 Pumice is merocrystalline with colorless anhedral mineral grains/clots of dark black, prismatic, sub-vitreous crystals within amorphous groundmass. The pumice shows variation in morphology from highly vesicular and brittle to dense and resistant. The vesicles are poly-modal and range in shape from elongate to circular and range from a few mm to a few cm in length. The vesicle density is moderate to high (Fig. 2A). Some samples of this pumice show compaction and flow texture. The

vesicles, unlike the samples of the SV-1, show lack of orientation. The larger vesicles appear to have formed from the coalescence of smaller vesicles. Deep-sea TV observation on the top of SM-1 volcano shows dull white to grey colored sheets of pumice capping on the surface, suggesting that these might have erupted without explosive volcanic activity (Rotella *et al.*, 2013).

The glass shows flow texture (Fig. 2B) that might have developed due to the flow of viscous glass before it is completely quenched, dragging and changing the morphology of the vesicles along with it. Porphyritic texture is prominently seen in the SM-1 with phenocrysts of plagioclase, green colored pleochroic hornblende showing typical cleavage pattern and in some places large plagioclase grains are clustered together and floating on a glassy groundmass depicting glomeroporphyritic texture (Fig.2C).

In SM-1 pumice, glass is the dominant phase (54.96%) followed by the phase of vesicles (38.55%) and mineral phases like plagioclase, hornblende, quartz & opaques, that occur as phenocrysts, consists of approximately 5.88%. Some of the plagioclase grains show typical zoning due to reaction failure (Fig. 2D). Of these minerals plagioclase is predominant (4.37%) followed by hornblende (0.77%), quartz (0.59%) and opaques (0.15%). Presence of clear phenocryst (Fmanik) is indicative of contemporaneous crystallization along with the hosted melt. Similar observation has been reported for quartz crystals (Roberge *et al.*, 2005) for the Bishop tuff rhyolites from Owens Valley, California, United States.

In addition, few isolated grains/ crystals of Ti-rich spinels, ilmenite, were observed within the glassy groundmass of SM-1 pumice. Few iron-rich hematitic crystals are also seen. These two minerals are from the differentiated magma before the eruption. These minerals are in solid solution at temperatures more than 1050⁰ C (Deer *et al.*, 1978).

SV-1

SV-1 Pumice shows holocrystalline texture showing the presence of both glass and crystals, with anhedral crystals, 1-2 mm in size. Vesicles are dense, elongated (5 - 8 mm longest axis) and show parallel to sub-parallel arrangement and are 3 to 4 mm circular (shortest axis). Usually pumice breaks along the long axis of the vesicles. Most vesicles contain glass filaments strewn across it, indicating the explosive nature of the eruption. The glass in pumice is the dominant phase and is dark greenish to locally black in color. Rare subhedral plagioclase phenocrysts (modal >0.05%) are present in most of the pumice samples. The near absence of any minerals suggest that the aphyric pumice lava was super-heated when erupted (Tamura *et al.*, 2003).

The vesicles are the second most dominant feature under the microscope after glass. The vesicles are mostly unimodal however, in few samples, size and shape of vesicles is polymodal and show a preferential orientation parallel to each other (Fig. 2F). The vesicles are elongated to circular in shape and appear to have pushed the glass during their formation. In another sample from SV-1, swirling of the vesicles is seen probably due to the flow of the glass along with the vesicles after the eruption, which could probably be of an effusive type. The modal analysis reveals that highest modal percentage is of glass (70.94%) followed by most dominant phase i.e. vesicles (29.76%) in SV-1 with the plagioclase (0.13%) constituting the sole mineral phase.

6. WHOLE ROCK GEOCHEMISTRY

The volcanic pumice samples from Andaman arc-back-arc system are characterized by >65 wt.% silica contents (Table 2) that testify the silicic nature of parent melt. Total alkali vs. silica (TAS) contents for the studied pumice samples classify them as rhyolites (Fig. 3A, after Le Bas *et al.*, 1986). K₂O vs. SiO₂ variations further qualify these rhyolites from SV-1 volcano as low K and from SM-1 volcano as medium K varieties (Fig.3B, after Le Maitre *et al.*, 1989). Variations in the K₂O concentrations with respect to SiO₂ distinctly implicate tholeiitic and calc-alkaline composition of precursor magmas for SV-1 and SM-1 rhyolitic pumice (Fig. 3B). The low K and medium K rhyolites share overall uniform major element chemistry in terms of restricted range of SiO₂ (73.7-77.6 wt.%), moderate Al₂O₃ (13-15 wt.%), extremely low TiO₂ (0.2-0.3 wt.%), MgO (0.4-0.7 wt.%), CaO (1.8-2.6 wt.%), MnO (0.1-0.2 wt.%) and P₂O₅ (0.04-0.06 wt.%). Total alkali content ranges from 5.7 to 7.01 wt.%. Na₂O (4.1-5.96 wt.%) > K₂O for low K (1.1 wt.%) and medium K (1.8-1.93 wt.%) samples.

Transitional trace elements like Ni, Co and Cr show extremely low concentrations for the low K and medium K rhyolitic pumice. Among large ion lithophile elements (LILE), the medium K rhyolitic pumice (SM-1) samples are characterized by higher abundances of Rb (41.91-47.31 ppm) and Ba (340.6-396ppm) relative to their low K (SV-1) counterparts (Rb: 21.43-25.52 ppm; Ba: 226.9-290ppm). High field strength element (HFSE) compositions reveal higher concentrations of Zr and Y for the low K rhyolites (Zr: 133-149 ppm, Y: 25.4-26.8 pm) than that of the medium K type (Zr: 81-88ppm, Y: 19.62-22.12 ppm). In contrast to this, the medium K rhyolites (U: 1.2-1.3 ppm, Th: 5.98-6.73 ppm) are characterized by relatively greater abundances of U and Th than that of the low K rhyolites (U: 0.90-0.97, Th: 3.81-4.3 ppm). Chondrite normalized REE profile (Fig.4) reflects pronounced LREE enrichment with relative MREE and HREE depletion. The low and medium K pumice uniformly exhibit strong LREE/MREE (La/Sm_N: 2.32-3.50) and LREE/HREE (La/Yb_N: 3.04-4.99) fractionation trends. However, MREE shows feeble fractionation over HREE (Gd/Yb_N:

0.90-0.93). Chondrite normalized REE patterns depict negative Eu anomalies (Eu/Eu^* : 0.74-0.93) thereby indicating fractionation of plagioclase in the mantle residue. Primitive mantle normalized incompatible trace element abundance patterns (Fig. 4) reflect distinct negative anomalies at Nb with positive anomalies for LILE and LREE collectively attesting to LILE-LREE enriched-HFSE depleted chemistry of the precursor magma. Primitive mantle normalized Th positive anomaly attributes to fluid-fluxed Th enrichment in the source mantle.

7. DISCUSSION

7.1 Tectonic Implications

Geochemical compositions of precursor magmas resulting into ultramafic- mafic-felsic volcanism are primarily governed by the tectonic setting and mantle source characteristics. Geochemical characters of modern volcanic rocks such as MORB, OIB and IAB are strongly controlled by their geodynamic conditions of eruption. High field strength elements (HFSE, such as, Nb, Ta, Zr) serve as reliable geochemical proxies to constrain the tectonic environments associated with magmatism in oceanic and continental realms. The REE and HFSE are least sensitive to alteration and their ratios have been successfully applied to distinguish different geodynamic conditions involved in the process of magmatism (Condie, 2001; Song *et al.*, 2008; He *et al.*, 2010). The studied rhyolitic pumice from both of the submarine volcanoes in Andaman subduction zone share comparable trace and REE characteristics marked by relatively low HFSE and high LILE concentrations thereby indicating an analogous tectonic setting for the eruptions. The low values of Ti, Nb; high values of Zr/Nb, Zr/Y (Table 2) and Rb abundances (>100ppm) and Y+Nb values (<100ppm) suggest island arc setting for both the submarine volcanoes (Pearce *et al.*, 1984; Foley and Wheller, 1990; Pal *et al.*, 2004). The enrichment of LILE (e.g. Rb Ba, Th, K and U) and depletion of HFSE (e.g. Zr, Hf, Nb, Y, Ti) relative to typical primitive mantle values, negative Nb-Ta, Zr-Hf anomalies, and positive Th anomalies (Fig. 4) for the studied rhyolitic pumice from SM-1 and SV-1 volcanoes are in compliance with the geochemical characteristics of magmas generated in subduction zone setting. LILE, LREE and HFSE compositions in terms of Ba/Nb vs. La/Nb (Fig. 5A), La/Yb vs. Th/Yb (Fig. 5B) and Ba/Yb vs Ta/Yb (Fig.5C) variations conform to intraoceanic arc affinity for these rhyolitic pumice. The studied samples further show a geochemical and tectonic coherence with the pumice from Okinawa trough of Izu-Bonin-Mariana arc system in the Pacific Ocean (Fig. 5C and Fig.5D). The pumice samples from SV-1 volcano are characterized by low K tholeiitic compositions with relatively low Rb (21-43-25.52 ppm), Ba (226.9-290.9 ppm), U (0.90-0.97 ppm), Th (3.81-4.3 ppm), Ba/Yb (78.5-96.3), Ba/Nb (84.2-109) with respect to the medium K calc alkaline pumice corresponding to SM-1 volcano (Rb: 41.91-47.31 ppm; Ba: 340.6-396.1 ppm; U:1.2-1.3ppm; Th:

5.98-6.73 ppm; Ba/Yb: 128.8-145.4; Ba/Nb: 135.75-145.96). The elevated abundances of LILE, U, Th with higher values for LILE/HFSE and LILE/HREE ratios in the SV-I pumice samples compared to their SM-1 counterparts can be accounted in terms of increasing influx of subduction-derived fluids containing fluid-mobile elements during different stages of subduction. Tholeiitic arc magmas are erupted during initial stages of subduction, while calc-alkaline nature of parent melts with gradually enhanced influx of slab-dehydrated fluids and subducted slab sediments commensurate with progressive increase subduction maturity. Nb vs. Y (Fig. 6A) and Rb vs. Y+Nb (Fig. 6B) plots for the rhyolitic pumice in this study distinctly correspond to the volcanic arc field thereby conforming to their eruptions in an arc regime.

7.2 Eruptive Style

The studied pumice samples from SM-1 and SV-1 volcanoes, forming a part of Andaman volcanic arc, have high percentage of vesicles (Table 1) indicating either volatile exsolution and/or steam explosivity. The morphology and density of these pumice reflect the rates of rising of bubbles, ascent and the discharge of magma (Houghton and Wilson, 1989). SM-1 samples show a high degree of interconnectivity of the vesicles. Complete interconnection of the vesicles could occur during explosive eruption, by thermal contraction during cooling of the pumice or perhaps by hydration of the glass (Whitham and Sparks, 1986). SV-1 pumice show elongated, parallel to sub parallel vesicles that are very closely spaced and mostly trimodal which are indicative of three vesiculation events: (a) in the magma chamber, (b) in the conduit and (c) as a result of explosive eruption of the pumice (Whitham and Sparks, 1986). The samples reflect phreatomagmatic eruptions of the submarine volcanoes SM-1 and SV-1, which are generally a consequence of thermal contraction instead of thermal expansion in other types of eruptions. The interaction of superhot magma with cool water results in highly explosive eruptions. The occurrence of explosive volcanism at deeper water levels is poorly understood and has been a controversial subject over the past few decades (Kokelaar and Busby, 1992; Fiske *et al.*, 2001). Cas and Wright (1987) suggested that it is improbable that explosive eruptions can occur at depths more than a few tens of meters, while others report caldera forming silicic volcanism occurring at considerable depths. Such explosive eruptions do exist (except in very deep waters) and are usually seen at island arc settings (Allen *et al.*, 2010; Fiske *et al.*, 2001; Stern, 2010; Resing *et al.*, 2011). The submarine volcanoes that are sampled have erupted in an explosive nature under the water column of greater than 1.5 km depth. However, recently, Rotella *et al.* (2013) have proposed a new volcanic type of eruption called as Tangaroan type where in eruption is not explosive but it produces vesicular siliceous pumice. The dry density of all samples range from 0.40 gm/cc to 0.81 gm/cc, both being less dense than sea water (1.035 gm/cc). To understand the

behavior of the pumice in the submarine environment we must consider however, not the dry density of the rock, but rather the wet/saturated density (Fiske *et al.*, 2001). The saturated density of the samples (i.e. pores filled with sea water) range from 1.2gm/cc to 1.5gm/cc, thus suggesting that they might have sunk immediately. Whitham and Sparks (1986) experimentally proved that hot pumice, when exposed to cold water immediately absorbed water through its vesicles and sank immediately. Kato (1987) further recognized that the volatiles that filled the vesicles are heated, and when exposed to cold water, they collapse causing further influx of the sea water into the rock. These factors along with the hydrostatic pressure of the water column above the submarine volcanoes would suggest saturation of pumice with seawater almost immediately after the eruption (White, 2003).

7.3 *Crystal Fractionation and Assimilation*

Pumice are predominantly made up of glass and vesicles with a subordinate amount of phenocrysts. The presence of porphyritic and glomero-porphyritic textures exhibited by few minerals within a glassy ground mass indicate a phase of crystallization and a phase of quenching. Petrographical studies of the pumice reveal a distinct difference in the vesicularity and the mineralogical compositions. The vesicles of pumice from SV-1 are elongated and show parallel to sub parallel alignment, while the SM-1 pumice show a great variation in shape, size and orientation of the vesicles. The SM-1 seamount shows the presence of phenocrysts of plagioclase, hornblende and quartz along with the presence of opaques. The zoned plagioclase from SM-1 pumice indicate two possible conditions, fresh magma influx in the chamber/magma mixing or crystallization during cooling; the former process results in reversed zoning and the later results in normal zoning of the plagioclase crystal (Pal *et al.*, 2007). Hornblende is common in medium to high K₂O content pumice. Its presence is important as it is stable only if the melt contains >3 wt. % of H₂O at pressures in excess of 0.1 to 0.2 GPa and therefore provides information on both H₂O content as well as depth of magma segregation (Winter, 2010). Major oxide contents suggest that the pumice under study are essentially rhyolitic and are rich in alkali and poor in Fe-Mg minerals, indicating that either the process of partial melting or fractional crystallization operated between the time of formation of melt and its extrusion on the ocean floor. The small negative Eu anomaly can be attributed to the removal of plagioclase, as Eu shows a deviation from +3 oxidation state to +2 under certain conditions of oxygen fugacity and replaces Ca in the plagioclase crystal structure. The presence of high amounts of Ba and Sr in relation to Rb and low Rb/Sr and Rb/ Ba ratios are consistent with predominant plagioclase rather than K rich feldspar fractionation. This is further supported by the presence of plagioclase phenocrysts observed in the specimens of SM-1 and also in SV-1 thereby suggesting that the crystallization of plagioclase commenced during the residence time of the silicic magma. Plots of

studied samples on Sr vs. Ba diagram (Fig. 7A) invoke role of assimilation of lower oceanic arc crust in the genesis of these rhyolites.

Hydrous basalt and / or andesite are plausible source rocks from which rhyolites could be produced by partial melting (Tamura, 2002). Simple fractionation, however, is not the answer for magmatism in oceanic island arcs (Nicholson *et al.*, 2004). Studies of silicic volcanism along the Izu-Bonin arc, Japan suggests that the partial melting of solidified calc-alkaline andesites within the crust generated rhyolites; these partially melted felsic melts, enriched with volatiles cause a caldera forming eruption of aphyric rhyolitic pumice (Tamura, 2002 and Shukuno *et al.*, 2006). The injection of mafic magma in the crustal magma chamber may trigger the eruption due to combined efforts of increased mass, heat and volatile input into the andesite (Zellmer and Turner, 2007) till then these volcanoes might be just erupting small amounts of ash and or gases as in fumarolic activity which has been suggested for Barren Island volcano by Sheth (2014). It can be envisaged that in Andaman subduction zone, at SV-1, simple partial melting of the calc-alkaline source resulted in the rhyolitic volcanism while at SM-1, the calc-alkaline source containing high H₂O content is partially melted, indicated by the presence of hornblende crystals. When the magma ponded under the volcanic arc (Tamura, 2002) the fractional crystallization of plagioclase within the silicic froth began. Change in the conditions of the chamber resulted in the explosive extrusion of the magma that was quickly quenched to form a pumice containing phenocrysts of plagioclase and hornblende.

7.4 Intraoceanic subduction signature and variable slab-mantle interaction

Rhyolites constitute an integral component of the tholeiitic to calc-alkaline basalt–andesite–dacite–rhyolite (BADR) association of convergent margin setting. A combination of magmatic processes such as influx of slab-derived fluids and melts into mantle wedge, wedge melting, assimilation of crustal materials by arc magma and magma mixing play a very significant role in the petrogenetic evolution of tholeiitic to calc-alkaline mafic to felsic magmas (Gao *et al.*, 2012; Guan *et al.*, 2012; Qi *et al.*, 2012; Yang *et al.*, 2013). Rhyolites commonly occur in intraoceanic arc, continental arc and continental rift settings and their geochemical features are attributed to different petrogenetic processes (Ayalew and Ishiwatari, 2011). Rhyolitic magmas in intraoceanic arc settings (e.g. Izu-Bonin arc) are inferred to be partial melts derived by dehydration melting of calc-alkaline andesites in upper to middle oceanic arc crust (Tamura and Tatsumi, 2002), whereas continental arc rhyolites (e.g. Mt. Wasso rhyolites of Japan) are generated by partial melting of metamorphosed basalts of thickened lower crust associated with fractional crystallization and crustal assimilation (Deering *et al.*, 2008). Continental rift zone rhyolites (e.g. rhyolites from Ethiopia) are interpreted as products of fractional crystallization and crustal contamination of basaltic magma derived by intracrustal melting

(Garland *et al.*, 1997). Oceanic arc rhyolites are interpreted to have geochemical compositions conformable with that of partial melts produced by dehydration-melting of calc-alkaline andesites at low-pressure (<7 kbar). The Izu-Bonin volcanic arc represents a modern-day intraoceanic convergent margin where generation of rhyolite magmas is triggered by dehydration melting of calc-alkaline, andesitic component of oceanic crust and this melting is influenced by influx of hot basaltic magma derived by subduction-processed mantle wedge melting (Straub and Zellmer, 2012; Manikyamba *et al.*, 2014a; b; c). Pumice from the Andaman island arc systems have a characteristic low Ti content along with depleted HFSEs and enriched LILE concentrations concomitant to typical ‘arc signature’ (Foley and Wheller, 1990). Trace and rare earth element data (Table 2) with chondrite normalized REE profile and primitive mantle normalized multi-element spider diagrams (Fig. 4) show that pumice from both volcanoes in this study show comparable geochemical trends endorsing a coherent mantle source and analogous magmatic processes that were active before and during eruption of these pumiceous lavas. The rhyolites from both SM-1 and SV-1 volcanoes in this study exhibit enrichment of LILE and LREE with depletion of HFSE relative to typical primitive mantle values which are in accordance with the geochemical characteristics of subduction zone magmas generated in arc settings. The trace and REE compositions of the studied volcanic rocks, marked by negative Nb-Ta anomalies, Ti depletion, Th/Ta >2, La/Nb >1.4, Nb/Y = 0.1–1, Nb/Th <10, Zr/Nb >10, La/Sm >1.5, and Nb/La <<1 (Table 2), exclude their association with mid-oceanic ridge, oceanic-island, or oceanic plateau settings and imply a subduction-related ocean–ocean convergence. Geochemical signatures of modern arc-related magmatism suggest that the Ba/Nb ratio is an effective geochemical proxy to evaluate the fluid/water content in the mantle source, while Ba/La can be used as a tracer for the total slab-derived input into the sub-arc mantle wedge (He *et al.*, 2017). The Ba/Nb ratios for the Andaman volcanic pumice, ranging from 84-146, corroborate the presence of hydrous minerals (e.g., phlogopite or amphibole) in the source region, and their Ba/La (18.5-24.25) ratios endorse subduction input in the source of the parent magmas (He *et al.*, 2017). Ba/Nb vs. La/Nb (Fig. 5A), La/Yb vs. Th/Yb (Fig. 5B) and Ba/Yb vs. Ta/Yb (Fig. 5C) plots attest to LILE-LREE enriched, HFSE depleted nature of the magmas parental to the studied rocks. This signature was inherited through fluid-controlled metasomatism of sub-arc mantle wedge driven by dehydration of subducted Indian oceanic lithosphere and influx of fluid mobile non-conservative large ion lithophile elements into the adjacent mantle with selective retention of fluid immobile conservative HFSE in the subducted slab. Thus, the generation of these felsic volcanic rocks is marked by contributions from subduction components and their LILE-LREE enrichment over HFSE is attributed to slab-dehydration, fluid infiltration and flux melting processes. Nd-Hf compositions of arc magmas reveal that in comparison with Hf, Nd behaves as a mobile element in slab-derived

fluids/melts. It has been suggested that subduction-metasomatized mantle wedge have increased concentrations of Nd compared to Hf. The LILE-LREE-HFSE systematics of the pumice marked by elevated abundances of Nd with Hf depletion manifested in terms of high Nd/Hf ratios (4.12-6.4) in combination with Ba/Nb, Ba/La, Ba/Yb, La/Sm, La/Yb, Th/Ce ratios conform to metasomatism of mantle wedge melts by addition of dehydrated fluids and sediments released from the subducted Indian ocean lithospheric slab.

HFSE ratios involving Nb, Th, and Yb provide significant insights into the genesis of volcanic rocks in different tectonic settings. Plots of studied rocks on Th/Yb vs. Ta/Yb (Fig. 5D) and Th/Yb vs. Nb/Yb (Fig. 7B) diagram reflect pronounced subduction input for their genesis in an oceanic arc environment and indicate their geochemical and tectonic coherence with Mariana arc and Okinawa trough magmatism in the Pacific Ocean. Mobility of Th over HFSE and HREE in fluids released by dehydration of subducted oceanic slab accounts for the elevated abundances of Th in the resultant arc magmas (Figs. 5D and 7B). Th/Ce ratios (>0.1) and LREE enrichment over HFSE and HREE particularly point towards contribution from the subducted sediments which are characteristic to island arc magmas. The plots of the studied rhyolitic pumice on Nb/Zr vs. Th/Zr diagram (Fig. 7C) suggest variable enrichment of mantle by subduction-derived fluids for resulting into the low K tholeiitic and medium calc-alkaline K types magmas which is correlatable with progressive intraoceanic subduction process. The studied volcanic rocks with high Ce/Nb (9.5-13.5 and low Th/Nb (1.4-2.7) reflect the involvement of a depleted MORB-type mantle (DMM) in their genesis. However, the low (Nb/La) and relatively high Th/Nb ratios in combination with enrichment in fluid-mobile, non conservative elements and depletion of fluid immobile, conservative elements attest to prominent contributions from subduction-derived components (SDC) in the mantle triggering metasomatic enrichment and melting process. Zr/Hf, Zr/Sm and Nb/Ta ratios have identified different mantle sources that are responsible for the generation of Cenozoic island arc lavas viz. (a) depleted MORB source in the sub-arc mantle wedge, (b) MORB like source with signatures of slab melts having rutile-eclogite residues of cold, deep slabs and (c) melts from hot shallow slabs having amphibole-garnet residue (Konig and Schuth, 2011; Manikyamba *et al.*, 2014 a, b). The Zr/Hf, Nb/Ta and Zr/Sm ratios for the studied rhyolitic pumice show higher Zr/Hf and Zr/Sm in conjunction with lower Nb/Ta values (Table 2) compared with the primitive mantle (Zr/Hf = 36, Nb/Ta = 17 and Zr/Sm = 25) implying subduction-driven metasomatism of depleted MORB like mantle source in the sub-arc mantle wedge through variable contributions from subduction components. Geochemical characteristics of convergent plate magmatism are also influenced by the subduction geometry and age of the subducting lithospheric slab. A global correlation between the age of subducting oceanic

lithosphere and the composition of arc magmas suggest that tonalities, trondhjemites, adakites and dacites having low Yb (<1.9 ppm) and Y (<18 ppm) contents are produced by partial melting of basaltic crust of the slab (eclogitic composition) with residual garnet during steep subduction of hot, young lithosphere (<30 Ma; Defant and Drummond, 1990; Defant *et al.*, 1992; Drummond *et al.*, 1996). In contrast to this, tholeiitic to calc-alkaline association of basalt–andesite–dacite–rhyolite (BADR) magmas have higher Yb (>2 ppm) and Y in the range of 20–25 ppm. These are derived by shallow subduction of older oceanic lithosphere (>30 Ma) with slab dehydration-wedge melting and wedge hybridization by melting of metamorphosed basaltic crust (low-Mg amphibolitic composition) of subducted oceanic slab without residual garnet. The studied rhyolites with Yb contents mostly ranging from 2.34 to 3.1 ppm and Y contents varying between 19.62 and 26.8 ppm are in compliance with subduction of older Indian oceanic lithosphere beneath a relatively younger Burmese an oceanic plate in the Northeastern Indian Ocean exemplifying an active ocean-ocean convergent plate margin with pronounced slab-mantle interaction, variable fluid-sediment flux into wedge mantle concurrent with progressive subduction processes resulting into oceanic arc rhyolites of low K tholeiitic to medium K calc-alkaline compositions . The Zr/Sm (24.9–42.8) and Nb/Ta (1.75–9.3) values for these rhyolites with respect to primitive mantle values (Zr/Sm: 25 and Nb/Ta: 17) reflect contributions from a depleted mantle wedge that was enriched and metasomatized by subduction-derived fluids and sediments in an intraoceanic arc setting.

7.5 Mantle-crust interaction and magma evolution

Magmas of intermediate to acidic compositions are generated and evolved through variable extents of mixing between crustal and mantle components. Partial melting of thickened crustal materials or solidified mafic magma stalled in the lower crust and fractional crystallization with or without crustal assimilation are the principal mechanisms that control the generation of rhyolite magmas in various tectonic settings (Ayalew and Ishiwatari, 2011). The principal mechanism for felsic magmatism in all kinds of tectonic settings include extraction of residual melt from crystal mushes during (i) partial melting within crust and/or (ii) crystallizing mush zones stalled in mid to lower crustal levels and fed by mafic-intermediate magmas. Melting processes in the mantle invoke two dominant lineage of magmatism and magma differentiation: (1) partial melting of mantle wedge in a subduction zone triggered by influx of fluids released from dehydrating subducted slab ensued by a cold, hydrous, oxidized differentiation trend of the resultant magma and (2) adiabatic decompressional melting of upwelling mantle in continental rift zones, intraplate hotspots and mid-oceanic ridge (MOR) settings with magma differentiation in a hot, dry and reduced regime. Silicic magmas generated under cold, wet, oxidizing environments in convergent plate margin settings show comparable major element

concentrations but distinct trace and REE chemistry with respect to those produced under hot, anhydrous, reducing conditions in hotspots, rift zones associated with continental and oceanic divergence. The REE profile for the Andaman rhyolitic pumice are analogous to wet rhyolites (Fig. 8; after Bachmann and Bergantz, 2008) and reflects a distinct fractionated pattern that may be attributed to sequestration of MREE by crystallization of amphibole in a cold, wet, oxidized domain associated with intraoceanic arc setting. Absence of negative Eu anomaly can be correlated with delayed plagioclase crystallization in hydrous environment. The evolution of magmas parental to the studied oceanic arc rhyolites from Andaman were controlled by fractionation of hydrous, oxidizing magmas carrying subduction-derived fluid and sediment influx and show clear distinction from rift-type felsic magmas involving fractionation of anhydrous, reducing melts (Christiansen, 2005; Deering *et al.*, 2008; Ayalew and Ishiwatari, 2011; Pankhurst *et al.*, 2011). The overall geochemical attributes for the submarine rhyolitic pumice from Andaman Sea suggest that they were erupted in an intraoceanic arc system and their petrogenesis involved (i) melting of mantle wedge fluxed with subduction components (ii) ascent of this melt, reheating, remobilization, partial melting and assimilation of andesitic component of lower oceanic crust and (iii) magma differentiation under cold, hydrous, oxidizing conditions in an oceanic arc regime.

8. Conclusions

- Submarine volcanic pumice dredged from SV-1 and SM-1 volcanoes of Andaman subduction zone are classified as low K and medium K oceanic arc rhyolites showing tholeiitic and calc-alkaline compositions respectively.
- Trace and REE compositions of these volcanic pumice corroborate strong subduction signatures in the parent melts that is reflected in elevated abundances for LILE-LREE with relative HFSE depletion. LILE-LREE enriched- HFSE depleted chemistry collectively suggest mantle wedge metasomatism by influx of slab-dehydrated fluids and sediments that transported the fluid mobile elements into the mantle, while the conservative, fluid immobile HFSE were retained in the dehydrated oceanic slab.
- Increased influx of slab-dehydrated fluids and subduction-derived components with subduction maturity account for the low K tholeiitic and medium K calc-alkaline compositions of rhyolitic pumice from SV-1 and SM-1 volcanoes respectively.
- Parental magmas evolved through under cold, hydrous oxidizing environments associated with convergent plate margin settings.

- Trace element signatures invoke subduction of older Indian oceanic lithosphere beneath a relatively younger Burmese oceanic plate in the Northeastern Indian Ocean with pronounced slab-mantle interaction and variable fluid-sediment flux into wedge mantle, resulting into mantle metasomatism.
- Petrogenetic aspects and tectonic implications (i) partial melting of mantle wedge fluxed with subduction-derived fluids and sediments (ii) ascent of this melt, reheating, remobilization, partial melting and assimilation of calc-alkaline andesitic component of lower oceanic crust (iii) magma differentiation under cold, hydrous, oxidizing conditions in an oceanic arc regime (iv) eruption of rhyolitic magma in an intraoceanic arc regime.
- The tectonic affinity and geochemical attributes for Andaman rhyolitic pumice are akin to those from Mariana arc and Okinawa Trough of Pacific Ocean and wet rhyolites of subduction zones thereby marking comparable intraoceanic subduction processes and magmatism operative in active, Phanerozoic ocean-ocean convergent margin settings.

Acknowledgement:

Authors are grateful to the Director, CSIR-National Institute of Oceanography for his encouragement, support and permission to publish this work. AS is thankful to Prof. M. Santosh for the invitation to contribute in the Special issue on Geological Journal. The authors thank two anonymous reviewers for their insightful suggestions which have greatly improved the quality of the manuscript. The authors acknowledge the funds from Council of Scientific and Industrial Research (CSIR) under MLP-1703 project. This is NIO's contribution No. XXXX.

References

- Allen, S. R., Fiske, R. S., Tamura, Y. 2010. Effects of water depth on pumice formation in submarine domes at Sumisu, Izu-Bonin arc, western Pacific. *Geology* 38, 391-394.
- Ayalew, D., Ishiwatari, A. 2011. Comparison of rhyolites from continental rift, continental arc and oceanic island arc: implication for the mechanism of silicic magma generation. *Island arc* 20, 78-93.
- Bachmann, O., Bergantz, G. W. 2008. Rhyolites and their source mushes across tectonic settings. *Journal of Petrology* 49, 2277-2285.
- Brown, D., 2009. The growth and destruction of the continental crust during arc-continent collision in the southern Urals. *Tectonophysics* 479, 185-196.
- Cas R.A.F., Wright, J.V. 1987. Volcanic successions modern and ancient. Allen & Unwin, London 528 P.

- Chen, C. H., Lee, T., Shieh, Y. N., Chen, C. H., Hsu, W. Y., 1995. Magmatism at the onset of back-arc basin spreading in the Okinawa Trough. *Journal of Volcanology & Geothermal Research* 69, 313-322.
- Christiansen, E. H. 2005. Contrasting processes in silicic magma chambers: Evidence from very large volume ignimbrites. *Geological Magazine* 142, 669-681.
- Condie, K. C. 2005. TTGs and adakites: are they both slab melts?. *Lithos* 80, 33-44.
- Condie, K. C. 1989. Geochemical changes in basalts and andesites across the Archean-Proterozoic boundary: identification and significance. *Lithos* 23, 1-18.
- Condie, K., 1993. Chemical composition and evolution of the upper continental crust: contrasting results from surface samples and shales. *Chem. Geol.* 104, 1-37.
- Curray, J. R. 2005. Tectonics and History of the Andaman Sea region. *Jour of Asian Earth Science* 25, 187-232.
- Curray, J. R., Moore, D. G., Lawver, L. A., Emmel, F. J., Raitt, R. W., Henry, M., Kieckhefer, R. 1979. Tectonics of the Andaman Sea and Burma. *Am. Assoc. Pet. Geol. Mem.* 29, 189-198.
- Deer, W.A., Howie, R.A., Zussman, J. 1978. An Introduction to the rock-forming minerals. Longman Pub., London 528 p.
- Deering, C. D., Cole, J. W., Vogel, T. A. 2008. A rhyolite compositional continuum governed by lower crustal source conditions in the Taupo Volcanic Zone, New Zealand. *Journal of Petrology*, 49 2245-2276.
- Defant, M. J., Drummond, M. S. 1990. Derivation of some modern arc magmas by melting of young subducted lithosphere. *Nature* 347, 662.
- Defant, M.J., Jackson, T.E., Drummond, M.S., De Boer, J.Z., Bellon, H., Feigemson, M.D., Maury, R.C., Stewart, R.H., 1992. The geochemistry of young volcanism throughout west Panama and southeastern Costa Rica: an overview. *Journal of Geological Society (London)* 149, 569-579.
- Drummond, M. S., Defant, M. J., Kepezhinskas, P. K. 1996. Petrogenesis of slab-derived trondhjemite-tonalite-dacite/adakite magmas. *Earth and Environmental Science Transactions of the Royal Society of Edinburgh* 87, 205-215.
- Fiske, R. S., Naka, J., Iizasa, K., Yuasa, M., Klaus, A. 2001. Submarine silicic caldera at the front of the Izu-Bonin arc, Japan; Voluminous seafloor eruptions of rhyolite pumice. *Geol. Society of Am Bulletin* 113, 813-824.
- Foley, S. F., G. E Wheller 1990. Parallels in the geochemical signatures of island arc volcanics and continental potassic igneous rocks: the role of residual titanites. *Chemical Geology* 85, 1-18.
- Foley, S. F., Wheller, G. E. 1990. Parallels in the geochemical signatures of island arc volcanics and continental potassic igneous rocks: the role of residual titanites. *Chemical Geology* 85, 1-18

- Gao, Y., Santosh, M., Hou, Z., Wei, R., Ma, G., Chen, Z., Wu, J., 2012. High Sr/Y magmas generated through crystal fractionation: evidence from Mesozoic volcanic rocks in the Northern Taihang orogen, North China Craton. *Gondwana Research* 22, 152-168.
- Garland, F., Hawkesworth, C.J., Mantovani, M.S.M. 1997. Reply to the comment by Harris and Milner on the paper 'description and petrogenesis of the Paraná rhyolites, southern Brazil' by Garland et al. (1995). *Journal of Petrology* 38, 299-302.
- Goss, A. R., Kay, S. M., Mpodozis, C. 2013. Andean adakite-like high-Mg andesites on the northern margin of the Chilean–Pampean flat-slab (27–28° S) associated with frontal arc migration and fore-arc subduction erosion. *Journal of Petrology* 54, 2193-2234.
- Guan, Q., Zhu, D. C., Zhao, Z. D., Dong, G. C., Zhang, L. L., Li, X. W., ... Yuan, H. L. 2012. Crustal thickening prior to 38 Ma in southern Tibet: evidence from lower crust-derived adakitic magmatism in the Gangdese Batholith. *Gondwana Research* 21, 88-99.
- Haldar, D., Laskar, T., Bandopadhyay, P.C., Sarkar, N.K., Biswas, J.K. 1992a. A note on the recent eruption of the Barren Island volcano. *Indian Minerals* 46, 77–88.
- Haldar, D., Luhr, J.F. 2003. The Barren Island volcanism during 1991 and 1994–95: eruptive style and lava petrology. *Geol. Soc. India Mem.* 52, 313–338.
- He, Q., Xiao, L., Balta, B., Gao, R., Chen, J. 2010. Variety and complexity of the late Permian Emeishan basalts: reappraisal of plume-lithosphere interaction process. *Lithos* 119, 91-107.
- He, X. F., Santosh, M., Ganguly, S. 2017. Mesozoic felsic volcanic rocks from the North China craton: Intraplate magmatism associated with craton destruction. *GSA Bulletin* 129, 947-969.
- Houghton, B. F., Wilson, C. J. N. 1989. A vesicularity index for pyroclastic deposits. *Bulletin of volcanology* 51, 451-462.
- Kamesh Raju, K. A. 2005. Three phase tectonic evolution of the Andaman backarc basin, *Current Science* 89, 1932-1936.
- Kamesh Raju, K. A., Ramprasad, T., Rao, P. S., Rao, B. R., Varghese, J. 2004. New insights into the tectonic evolution of the Andaman basin, northeast Indian Ocean. *Earth and Planetary Science Letters* 221, 145-162.
- Kamesh Raju, K.A., Ray, D., Mudholkar, Abahy.V., Murty, G.P.S., Gahalaut, V.K., Samudrala, K., Paropkari, A.L., Ramachandran, R., Surya Prakash, L. 2012. Tectonic and volcanic implications of a cratered seamount off Nicobar Island, Andaman Sea. *J Asian Earth Sci.* 56, 42-53.
- Kato, Y., 1987. Woody pumice generated with submarine eruption. *Journal of the Geological Society of Japan* 77, 193–206.
- Kokelaar, P., Busby, C. 1992. Subaqueous explosive eruption and welding of pyroclastic deposits. *Science* 257, 196-20.
- König, S., Schuth, S. 2011. Deep melting of old subducted oceanic crust recorded by superchondritic Nb/Ta in modern island arc lavas. *Earth and Planetary Science Letters* 301, 265-274.

- Le Bas M., Maitre, R. L., Streckeisen, A., Zanettin, B. 1986. IUGS Subcommittee on the Systematics of Igneous Rocks 1986. A chemical classification of volcanic rocks based on the total alkali-silica diagram. *Journal of Petrology* 27, 745-750
- Le Maitre R.W. (Ed.), 2002. *Igneous Rocks: A Classification and Glossary of Terms. Recommendations of the International Union of Geological Sciences Subcommittee on the Systematics of Igneous Rocks*, Cambridge University Press, Cambridge, 236 pp.
- Le Roux, A.P., 1986. Geochemical correlation between southern African kimberlites and south Atlantic hotspots. *Nature* 324, 243–245
- Leat, P. T., Larter, R. D. 2003. Intra-oceanic subduction systems: introduction. *Geological Society, London, Special Publications* 219, 1-17.
- Lodolo, E., Coren, F., Ben-Avraham, Z. 2013. How do long-offset oceanic transforms adapt to plate motion changes? The example of the Western Pacific-Antarctic plate boundary. *Journal of Geophysical Research: Solid Earth* 118, 1195-1202.
- Manikyamba, C., Saha, A., Santosh, M., Ganguly, S., Singh, M. R., Subba Rao, D.V., 2014a. Neoproterozoic felsic volcanic rocks from the Shimoga greenstone belt, Dharwar Craton, India: geochemical fingerprints of crustal growth at an active continental margin. *Precambrian Research* 252, 1-21.
- Manikyamba, C., Ganguly, S., Saha, A., Santosh, M., Singh, M. R., Subba Rao, D.V., 2014b. Continental lithospheric evolution: constraints from the geochemistry of felsic volcanic rocks in the Dharwar Craton, India. *Journal of Asian Earth Sciences*. DOI: 10.1016/j.jseas.2014.05.020.
- Manikyamba, C., Saha, A., Ganguly, S., Santosh, M., Lingadevaru, M., Singh, M. R., Rao, D. S. 2014c. Sediment-infill volcanic breccia from the Neoproterozoic Shimoga greenstone terrane, western Dharwar Craton: Implications on pyroclastic volcanism and sedimentation in an active continental margin. *Journal of Asian Earth Sciences* 96, 269-278.
- Maruyama, S., Hasegawa, A., Santosh, M., Kogiso, T., Omori, S., Nakamura, H., Kawai, K., Zhao, D., 2009. The dynamics of big mantle wedge, magma factory, and metamorphic–metasomatic factory in subduction zones. *Gondwana Research* 16, 414-430.
- Nicholson, K. N., Black, P. M., Hoskin, P.W. O., Smith, E. M. 2004. Silicic volcanism and back arc extension related to the migration of the late Cenozoic Australian Pacific plate boundary. *Journal of Volcanology and Geothermal Research* 131, 295-30
- Pal, T., Chakraborty, P. P., Gupta, T. D., Singh, C. D. 2003. Geodynamic evolution of the outer-arc–forearc belt in the Andaman Islands, the central part of the Burma–Java subduction complex. *Geological Magazine* 140, 289-307.
- Pal, T., Gupta, T. D., Chakraborty, P. P., Das Gupta, S. C. 2004. Pyroclastic deposits of Miocene age in the ArakanYoma-Andaman-Java subduction complex, Andaman Islands, Bay of Bengal, India. *Geochemical Journal* 39, 69-82.

- Pal, T., Mitra, S.K., Sengupta, S., Katari, A., Bandopadhyay, P.C., Bhattacharya, A.K. 2007. Dacite-andesites of Narcondam volcano in the Andaman Sea — an imprint of magma mixing in the inner arc of the Andaman–Java subduction system. *Journal of Volcanology and Geothermal Research* 168, 93–113.
- Pankhurst, M. J., Schaefer, B.F., Betts, P.G. 2011. Geodynamics of rapid voluminous felsic magmatism through time. *Lithos* 123, 92-101.
- Pearce, J.A. 2008. Geochemical fingerprinting of oceanic basalts with applications to ophiolite classification and the search for Archean oceanic crust. *Lithos* 100, 14-48.
- Pearce, J. A., Harris, N. W., Tindle, A. G., 1984. Trace element discrimination diagrams for the tectonic interpretation of granitic rocks. *Journal of Petrology* 25 956 – 983
- Pearce, J. A., Stern, R. J., Bloomer, S. H., Fryer, P. 2005. Geochemical mapping of the Mariana arc-basin system: Implications for the nature and distribution of subduction components. *Geochemistry Geophysics Geosystems* 6, 542-557.
- Qi, X., Zeng, L., Zhu, L., Hu, Z., Hou, K., 2012. Zircon U-Pb and Lu-Hf isotopic systematics of the Daping plutonic rocks: implications for the Neoproterozoic tectonic evolution of the northeastern margin of the Indo-China block, Southwest China. *Gondwana Research* 21, 180-193.
- Rao, P. S., Kamesh Raju, K. A., Ramprasad, T., Nagendra Nath, B., Ramalingaswara Rao, B., Rao, Ch. M., Nair, R.R. 1996. Evidence for hydrothermal activity in the Andaman back arc basin. *Current Science* 70, 379-385.
- Ray, D., Rajan, S., Ravindra, R. 2012. Role of subducting component and sub-arc mantle in mantle petrogenesis: Andaman volcanic arc. *Current Science* 102, 605-609
- Resing, J. A., Rubin, K.H., Embley, R.W., Lupton, J.E., Edward T. Baker, E.T., Dziak, R.P., Baumberger, T., Marvin D. Lilley, M.D., Huber, J.A., Shank, T.A., Butterfield, D. A. Clague, D.A., Nicole S. Keller, N.S., Merle, S.G., Nathaniel J. Buck, N.J., Michael, P.J., Soule, S., Caress, D.W., Walker, S.L. Davis, R., Cowen, J.P. Anna-Louise Reysenbach, A-L., Thomas, H. 2011. Active submarine eruption of boninite in the northeastern Lau Basin. *Nature Geoscience* 4, 799-806.
- Roberge, J., Wallace, P.J., Kent A.A., 2005. The Origin of quartz phenocrysts in the Bishop tuff rhyolitic magma based on trace elements in melt inclusions and pumice matrix glass. AGU Fall meeting Abstract#V13B-0524.
- Rodolfo, K.S., 1969. Bathymetry and marine geology of the Andaman basin and tectonic implications for SE Asia, *Geol. Soc. Am. Bull.* 80, 1203-1230.
- Rotella, M.D., Wilson, C.J.N., Barker, S.J., Wright, I.C. 2013. Highly vesicular pumice generated by buoyant detachment of magma in subaqueous volcanism. *Nature Geoscience* 6, 129-132
- Roy, S. K., 1992. Accretionary Prism in Andaman Forearc. *Geol. Surv. Ind. Spl. Pub. No. 29*, 273-278.

- Saha, A., Dhang, A., Ray, J., Chakraborty, S., Moecher, D., 2010. Complete preservation of ophiolite suite from south Andaman, India: A mineral-chemical perspective. *Journal of Earth System Science*. 119, 365-381
- Saha A., Mudholkar, A.V., Kamesh Raju, K. A., Doley, B., Sensarma, S. 2018a Geochemical characteristics of basalts from Andaman subduction zone: Implications on magma genesis at intraoceanic back arc spreading centres. *Geological Journal*. DOI: 10.1002/gj.3345
- Saha, A., Santosh, M., Ganguly, S., Manikyamba, C., Ray, J., Dutta, J. 2018b. Geochemical cycling during subduction initiation: evidence from serpentinized mantle wedge peridotite in the south Andaman ophiolite suite. *Geoscience Frontiers* 9, 1755-1775.
- Sheth H. 2014. What drives centuries-long polygenetic scoria cone activity at Barren Island volcano? *Journal of Volcanology and Geothermal Research* 289, 64-80.
- Sheth, H.C., Ray, J.S., Bhutani, R., Kumar, A., Awasthi, N., 2010. The latest (2008–09) eruption of Barren Island volcano, and some thoughts on its hazards, logistics and geotourism aspects. *Current Science* 98, 620–626.
- Sheth, H.C., Ray, J.S., Bhutani, R., Kumar, A., Smitha, R.S., 2009. Volcanology and eruptive styles of Barren Island: an active mafic stratovolcano in the Andaman Sea, NE Indian Ocean. *Bull. Volcanol.* 71, 1021–1039.
- Sheth, H.C., Ray, J.S., Kumar, A., Bhutani, R., Awasthi, N., 2011. Toothpaste lava from the Barren Island volcano (Andaman Sea). *Journal of Volcanology and Geothermal Research* 202, 73–82.
- Shinjo, R., Chung, S. L., Kato, Y., and Kimura, M., 1999. Geochemical and Sr-Nd isotopic characteristics of volcanic rocks from the Okinawa Trough and Ryukyu arc: Implications for the evolution of a young, intra-continental back arc basin. *Journal of Geophysical Research: Solid Earth* 104, 10591-10608.
- Shinjo, R., Kato, Y., 2000. Geochemical constraints on the origin of bimodal magmatism at the Okinawa Trough, an incipient back-arc basin. *Lithos* 54, 117-137.
- Shukuno, H., Tamura, Y., Tani, K., Chang, Q., Suzuki, T., Fiske, R. S. 2006. Origin of silicic magmas and compositional gap at Sumisu submarine caldera, Izu- Bonin arc, Japan. *Journal of Volcanology and Geothermal Research* 156, 187-216.
- Song, X-Y., Qi, H-W., Robinson, P.T., Zhou, M-F., Cao, Z-M., Chen L-M. 2008. Melting of the subcontinental lithospheric mantle by the Emeishan mantle plume; evidence from the basal alkaline basalts in Dongchuan, Yunan, Southwestern China. *Lithos* 100, 93-111.
- Stern, C. R. 1991. Role of subduction erosion in the generation of Andean magmas. *Geology* 19, 78-81.
- Stern, R. J. 2010. The anatomy and ontogeny of modern intra-oceanic arc systems. Geological Society, London, Special Publications 338, 7-34.
- Straub, S.M., Zellmer, G.F. 2012. Volcanic arcs as archives of plate tectonic change. *Gondwana Research* 21, 495-516.

- Subrahmanyam, C., Gireesh, R., Chand, Shyam., Kamesh Raju, K.A., Gopala Rao, D. 2008. Geophysical characteristics of the Ninetyeast Ridge–Andaman Island arc/ trench convergent zone. *Earth and Planetary Science Letters* 266, 29–45.
- Sun, S.S., McDonough, W.F. 1989. Chemical and isotopic systematics of oceanic basalts: implications for mantle composition and processes. In: Saunders, A.D., Norry, M.J. (Eds.), *Magmatism in the Ocean Basins*. Geological Society Special Publication, London, pp. 313–345.
- Tamura, Y., Tatsumi, Y., 2002. Remelting of an Andesitic Crust as a possible origin for rhyolitic magma in Oceanic arcs: An Example from the Izu-Bonin Arc. *Journal of Petrology* 43, 1029–1047.
- Tamura, Y. 2002. Silicic volcanism and plutonism in the IBM arc. NSF-IFREE MARGINS, Subduction Factory Workshop.
- Tamura, Y., Yuhara, M., Ishii, T., Irino, N., Shukuno, H. 2003. Andesites and Dacites from Daisen Volcano, Japan: Partial-to-Total Re-melting of an Andesite Magma Body. *Journal of Petrology* 44, 2243–2260.
- White, J.D.L., Smellie, J.L., Clague, J.L. 2003. Introduction: A deductive outline and topical overview of subaqueous explosive volcanism. *Explosive Subaqueous Volcanism*, AGU Geophysical Monograph 140, 1–23.
- Whitham, A. G., Sparks, R. G. S. 1986. Pumice. *Bulletin of Volcanology* 48, 209–223.
- Winter, J. D. 2010. *Principles of Igneous and Metamorphic Petrology*. Second Edition. Pearson Prentice Hall Publications.
- Yang, Q.Y., Santosh, M., Shen, J.F., Li, S.R., 2013. Juvenile vs. recycled crust in NE China: Zircon U–Pb geochronology, Hf isotope and an integrated model for Mesozoic gold mineralization in the Jiaodong Peninsula. *Gondwana Research*, <http://dx.doi.org/10.1016/j.gr.2013.06.003>.
- Zellmer, G. F., Turner, S.P. 2007. Arc dacite genesis pathways: evidence from mafic enclaves and their hosts in Aegean lavas. *Lithos* 95, 346–362.
- Zhao, J.J., Zhou, M.F. 2007. Geochemistry of Neoproterozoic mafic intrusions in the Panzhihua district (Sichuan Province, SW China): implications for subduction related metasomatism in the upper mantle. *Precambrian Research* 152, 27–47.

Figure Caption

Figure 1.

- A. Regional geology of Andaman Basin with all important tectonic and geomorphic features present within basin.
- B. Detail multi-beam bathymetry of SM-1 volcano
- C. Detail multi-beam bathymetry of SV-1 volcano

Figure 2. (A) Scanning Electron Microscope (SEM) photograph showing the mesh pattern formed by the vesicles in rhyolitic pumice (B) Photomicrograph showing the primary flow texture in the pumice (C) Photomicrograph showing oscillatory zoning in plagioclase phenocryst in rhyolitic pumice (D) Photomicrograph showing oscillatory zoning in plagioclase phenocryst (E) SEM photograph showing the occurrence of crystalline quartz in pumice (F) Photomicrograph showing parallel orientation of elongated vesicles in rhyolitic pumice

Figure 3.

- A. Total alkali vs. silica diagram for the rhyolitic pumice from Andaman back arc basin (after LeBas *et al.*, 1986)
- B. K₂O vs. SiO₂ variations depicting a medium and low K affinity for studied samples from SM-1 and SV-1 respectively (after Le Maitre *et al.*, 1989)

Figure 4.

Chondrite normalized REE patterns and primitive mantle normalized multi-element spider diagram for the studied samples (normalization values are from Sun and McDonough, 1989)

Figure 5.

- A. Ba/Nb vs. La/Nb diagram for the studied samples showing arc affinity. Data sources for other fields: PM: primitive mantle (Sun and McDonough, 1989); CC: continental crust and Clastic sediment average (Condie, 1993); MORB, OIB and Dupal OIB (Le Roux, 1986)
- B. Plots of studied samples showing intra oceanic arc affinity in La/Yb vs. Th/Yb diagram (after Condie 1989)
- C. and D. Plots of studied samples from the Andaman basin in Ba/Yb and Th/Yb vs Ta/Yb diagram. The figure is modified from Pearce *et al.*(2005) and Chen *et al.* (1995). Data of Okinawa Trough basalt cited from Shinjo *et al.* (1999), is average; data of N-MORB, E-MORB and primitive mantle are cited from Sun and McDonough (1989); data of Okinawa Trough pumice from Shinjo and Kato (2000); data of Mariana trough basalt from Pearce *et al.* (2005)

Figure 6.

Plots of studied corresponds to volcanic arc field in (A) Nb vs Y and (B) Rb vs. Y+Nb discrimination diagrams (Pearce *et al.*, 1984)

Figure 7.

- A. Plots of studied samples on Sr vs. Ba diagram.
- B. Th/Yb vs. Nb/Yb plots for the studied samples showing calc-alkaline lineage in intra oceanic arc domain (Pearce, 2008).
- C. Nb/Zr vs. Th/Zr diagram (after Zhao and Zhou, 2007) showing the studied samples in an array consistent with fluid-related enrichment of mantle through subduction process

Figure 8.

Chondrite normalized REE patterns (Avg.) for rhyolitic pumice from SM-1 and SV-1 volcanoes. Background REE patterns for the two types of high-SiO₂ rhyolite (cold-wet-oxidized and hot-dry-reduced) adopted from Bachmann and Bergantz, 2008.

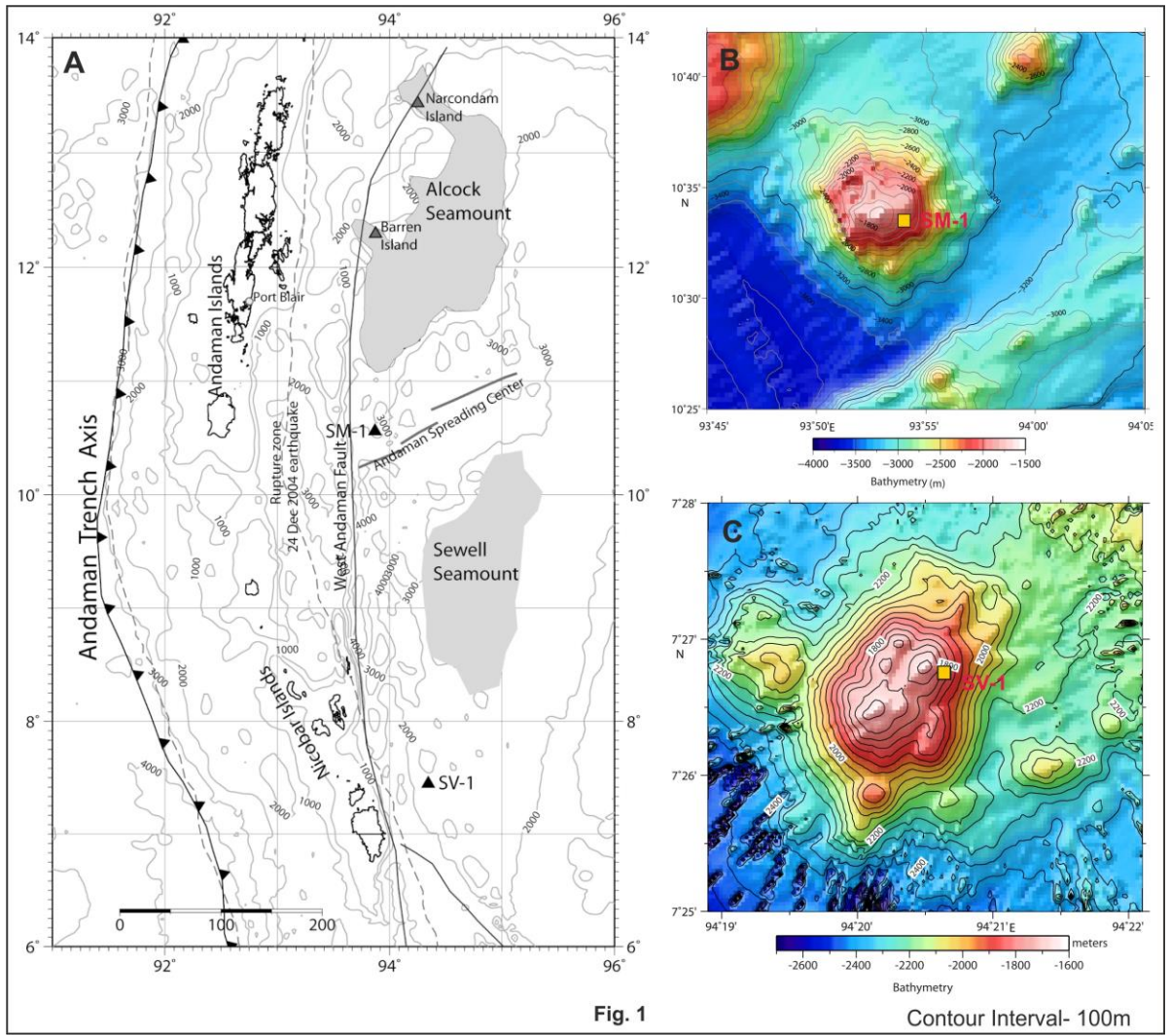


Fig. 1

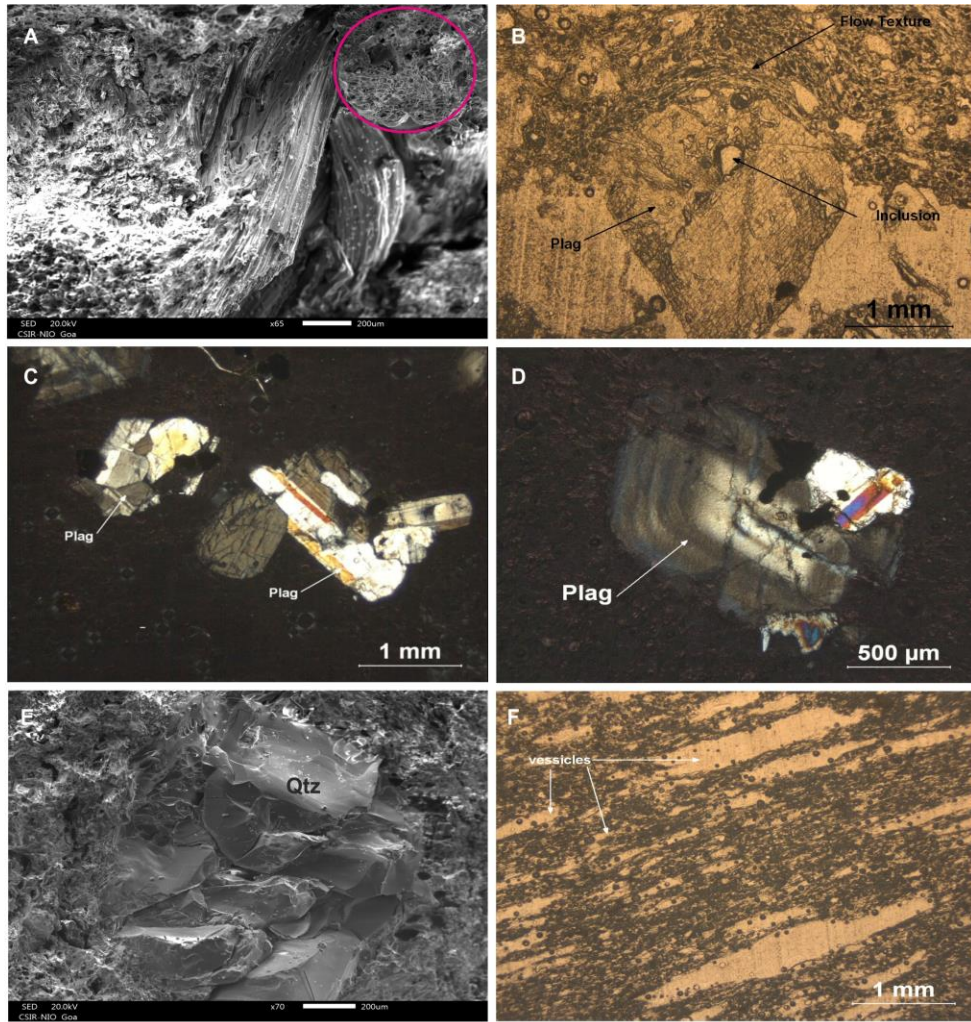


Fig. 2

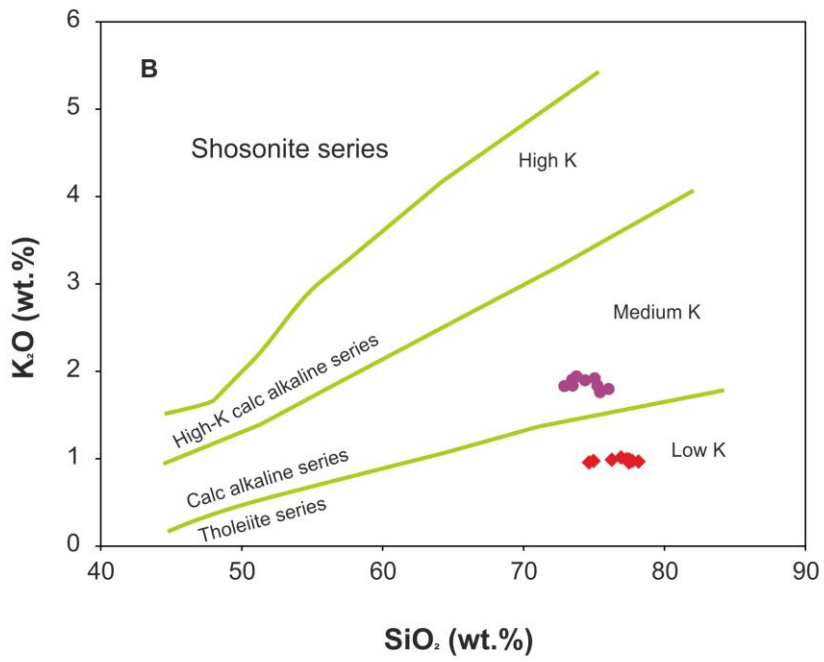
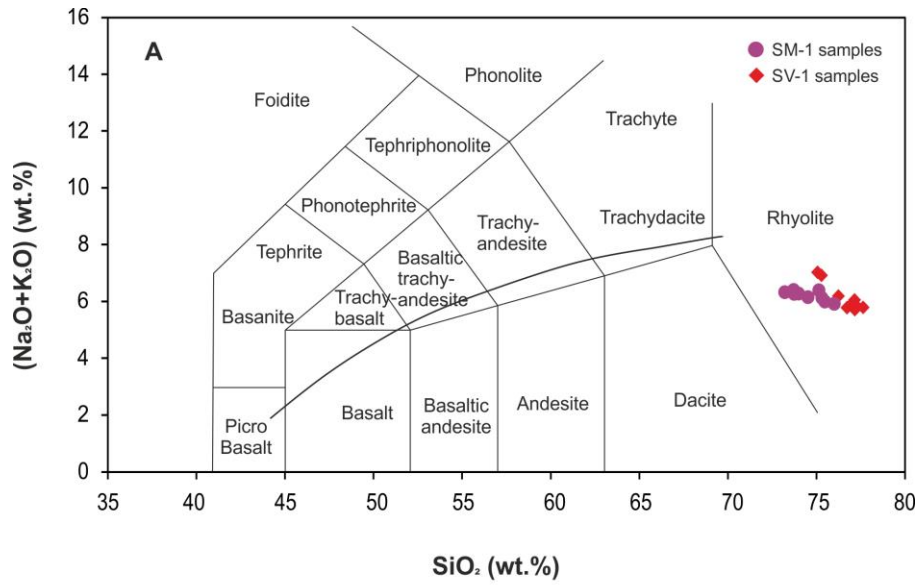


Fig. 3

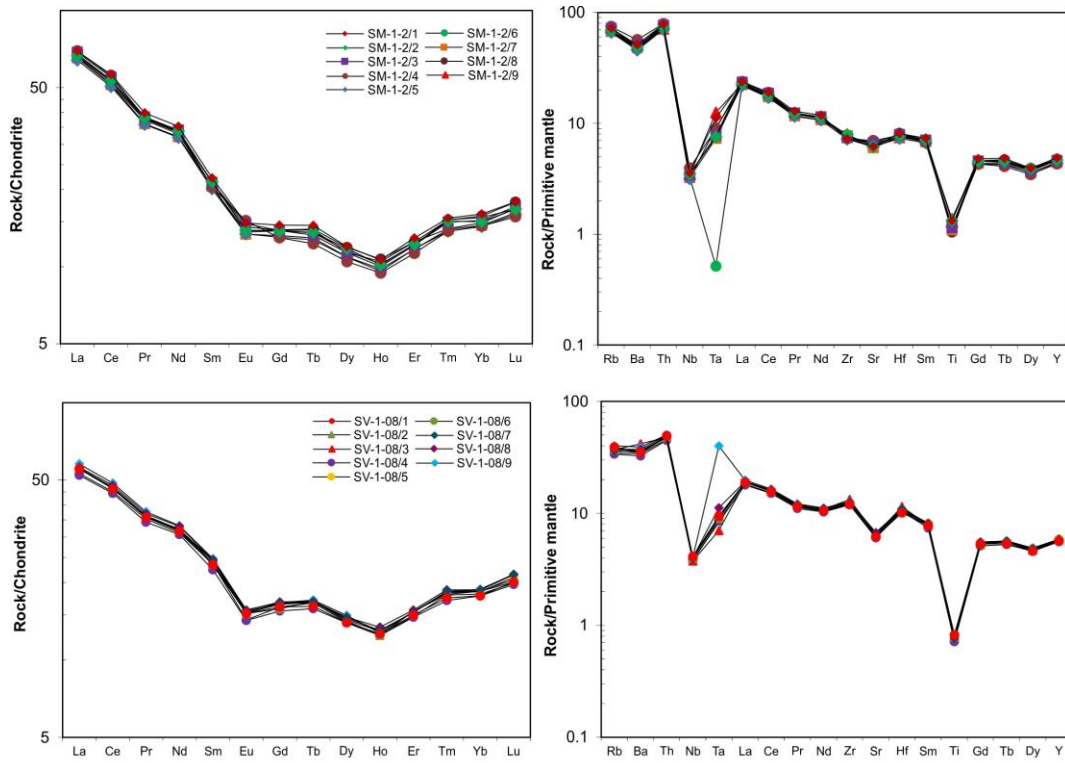


Fig. 4

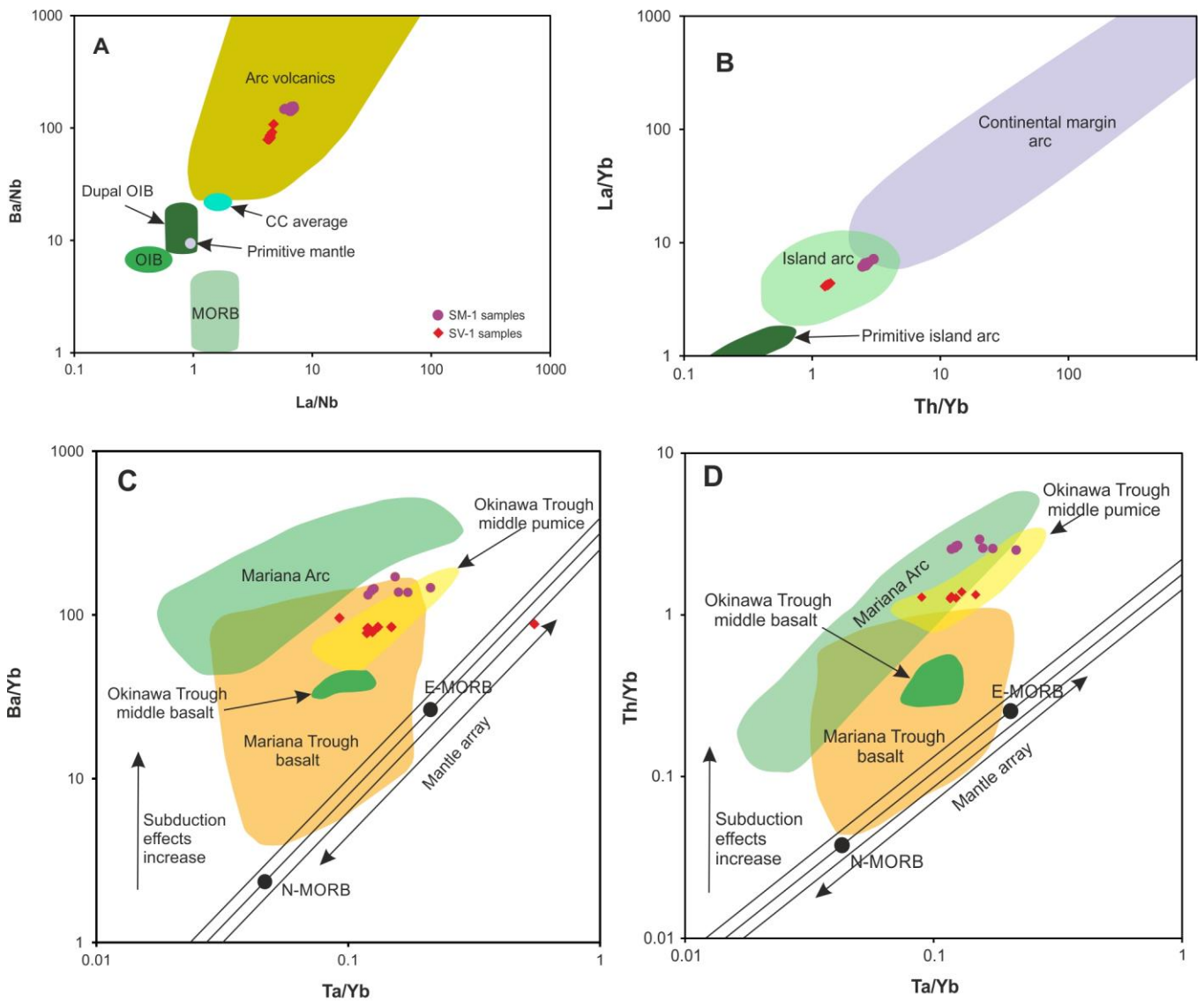


Fig. 5

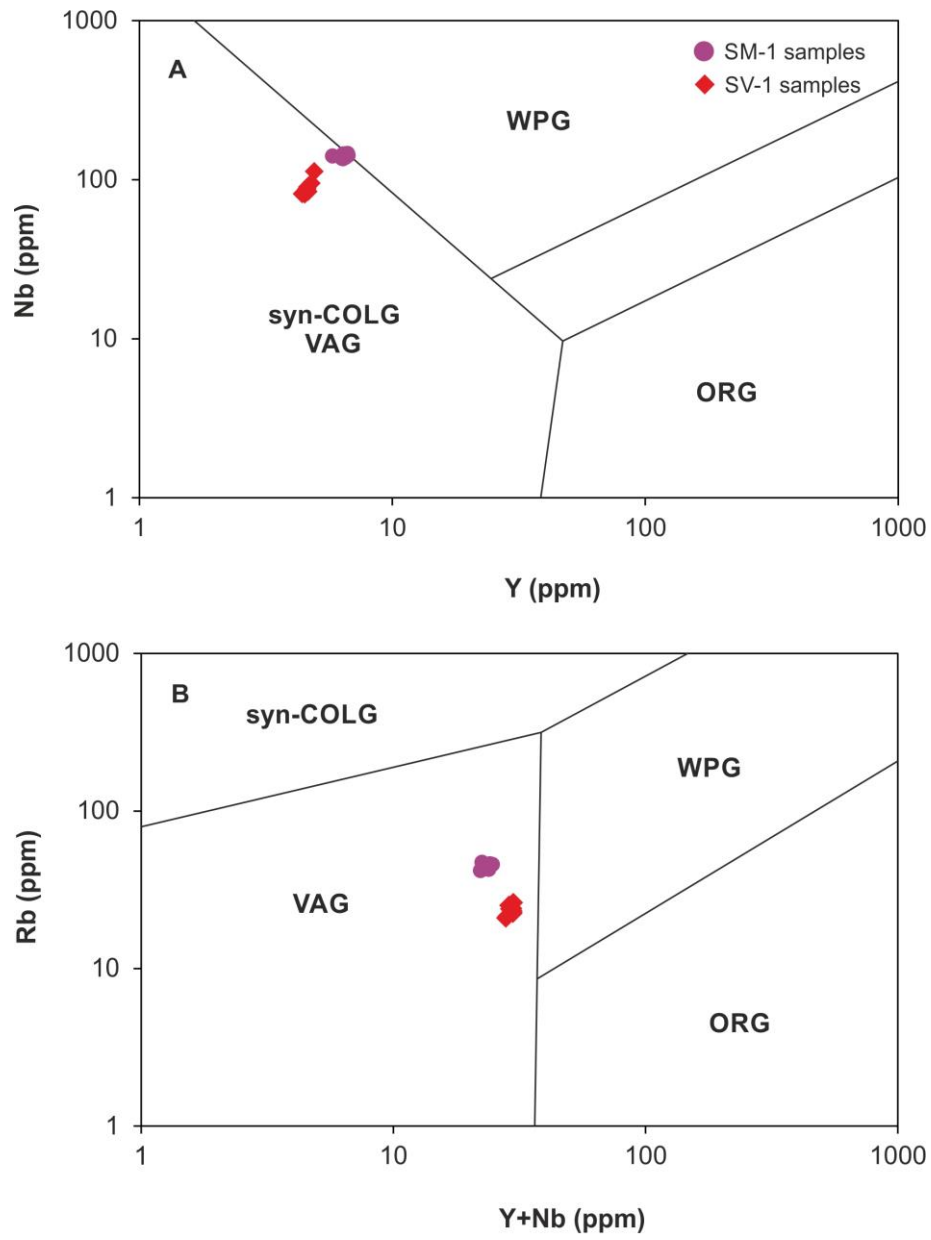


Fig. 6

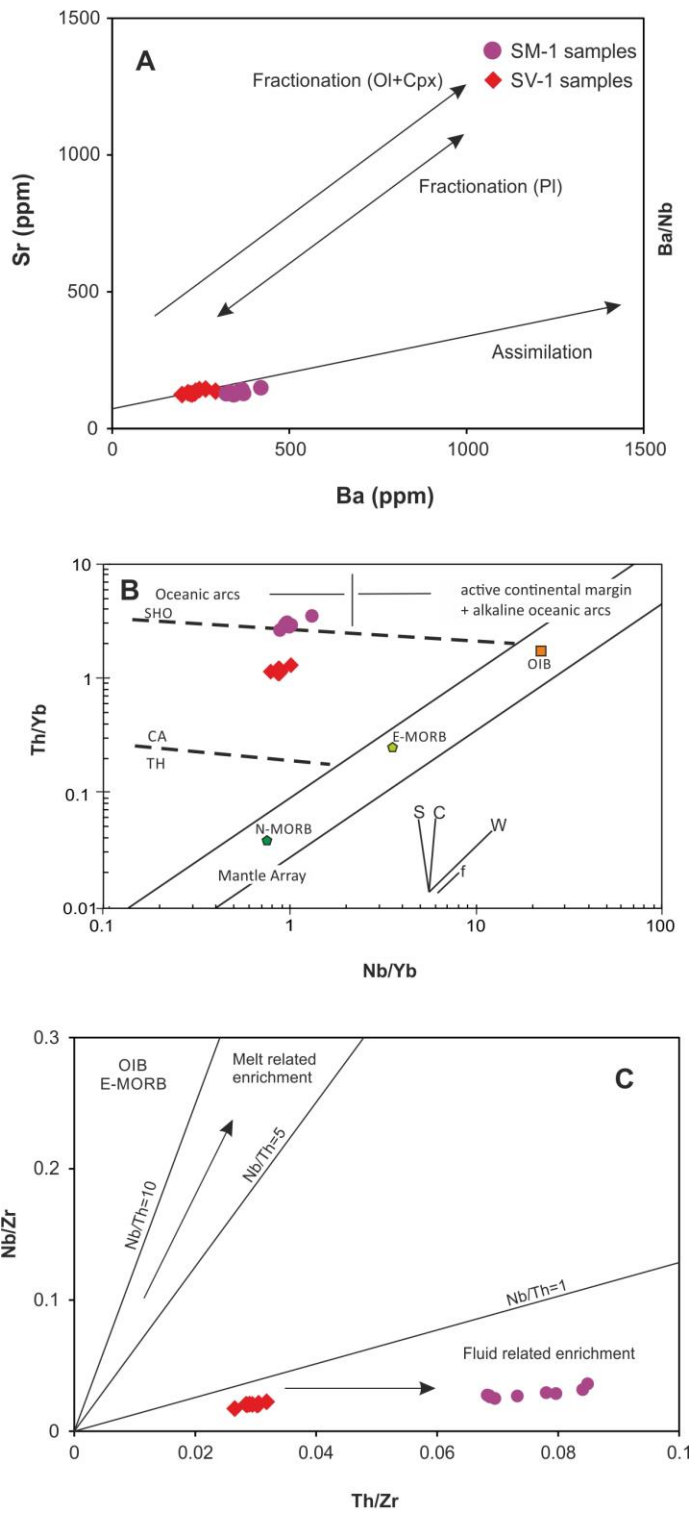


Fig. 7

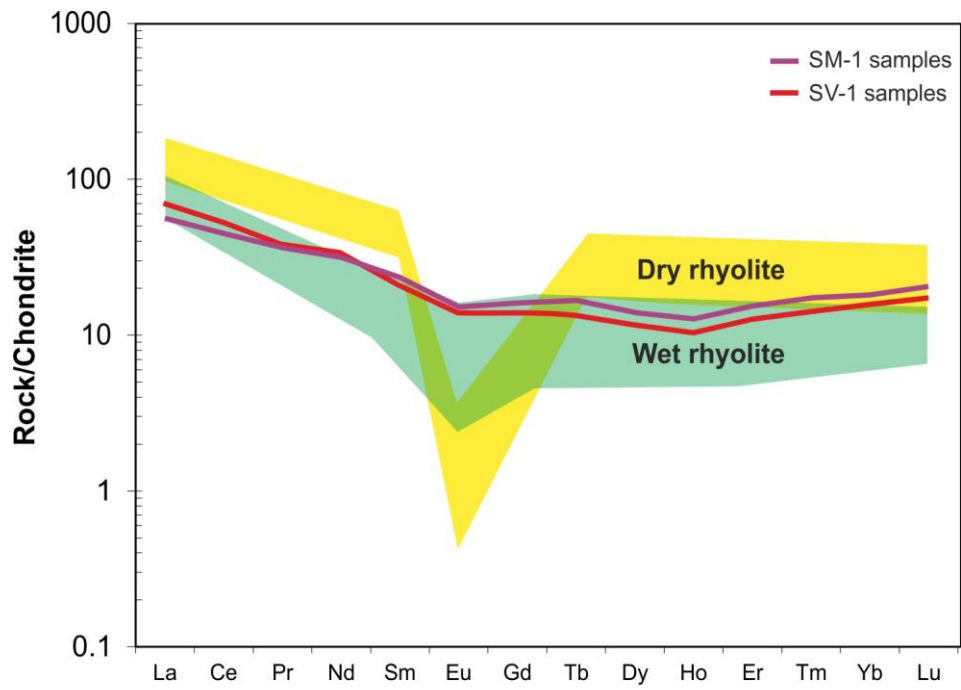


Fig. 8

Table 1 Physical properties of rhyolitic pumice from SM-1 and SV-1

	SM-1	SV-1	
Physical properties	Specific Gravity	2.280	1.845
	Dry Density	0.813	0.407
	Porosity	60.100	77.470
	Saturated density	1.500	1.207

Table 2 Major and trace element composition of rhyolitic pumice from Andaman back arc basin

wt. %	SM-1-2 /1	SM-1-2 /2	SM-1-2/3	SM-1-2/4	SM-1-2/5	SM-1-2 /6	SM-1-2/7	SM-1-2/8	SM-1-2/ 9
SiO ₂	73.94	75.43	73.66	73.69	75.26	74.47	75.95	75.09	73.16
TiO ₂	0.29	0.29	0.25	0.26	0.25	0.25	0.24	0.23	0.30
Al ₂ O ₃	14.39	13.75	14.93	14.97	13.82	14.25	13.48	14.37	14.42
FeO	2.28	2.20	1.93	2.12	1.88	1.98	1.89	1.98	2.26
MnO	0.10	0.10	0.09	0.10	0.08	0.08	0.13	0.08	0.11
MgO	0.64	0.66	0.53	0.62	0.56	0.58	0.51	0.55	0.69
CaO	2.39	2.36	2.56	2.55	2.31	2.48	2.29	2.35	2.57
Na ₂ O	4.33	4.20	4.49	4.41	4.26	4.24	4.10	4.46	4.48
K ₂ O	1.93	1.77	1.90	1.84	1.84	1.89	1.81	1.91	1.83
P ₂ O ₅	0.06	0.05	0.05	0.05	0.05	0.05	0.05	0.04	0.06
Total	100.34	100.81	100.39	100.60	100.31	100.27	100.43	101.05	99.87
Na ₂ O+K ₂ O	6.27	5.98	6.39	6.25	6.10	6.13	5.90	6.37	6.31
<i>ppm</i>									
Cr	6.86	7.22	6.50	7.90	5.34	7.56	7.54	7.36	8.29
Co	4.47	4.69	4.07	4.76	3.77	4.17	5.88	3.87	4.57
Ni	3.26	3.36	3.82	4.06	2.15	2.86	4.61	3.38	4.09
Rb	46	44	46	47	42	43	43	46	43
Sr	130	132	141	147	129	135	127	128	140
Cs	1.69	1.59	1.74	1.89	1.47	1.52	1.55	1.60	1.59
Ba	358	341	354	396	320	327	336	338	352
Sc	5.02	4.86	4.37	3.96	4.33	4.94	4.12	4.61	5.05
V	41.17	36.68	28.04	29.12	31.91	31.14	28.47	24.77	32.74
Ta	0.46	0.31	0.32	0.37	0.37	0.02	0.30	0.31	0.51
Nb	2.56	2.49	2.43	2.81	2.25	2.35	2.30	2.49	2.42
Zr	81.26	88.26	83.04	81.69	80.56	85.51	86.61	83.59	85.28
Hf	2.50	2.38	2.46	2.41	2.26	2.33	2.34	2.51	2.30
Th	6.65	6.26	6.54	6.73	5.98	6.07	6.20	6.49	6.03
U	1.30	1.21	1.29	1.26	1.19	1.22	1.24	1.30	1.23
Y	22.12	21.25	21.01	19.62	19.91	21.49	20.26	21.62	21.24
La	16.31	15.67	16.14	16.33	15.05	15.37	15.33	15.87	15.51
Ce	33.91	32.12	33.12	33.62	30.41	31.11	30.93	32.23	31.71
Pr	3.55	3.38	3.41	3.39	3.19	3.33	3.22	3.41	3.36
Nd	15.96	15.26	15.44	15.26	14.42	14.92	14.53	15.22	15.12
Sm	3.27	3.15	3.14	3.01	2.96	3.03	3.02	3.15	3.14
Eu	0.83	0.78	0.82	0.85	0.75	0.76	0.75	0.77	0.80
Gd	2.86	2.71	2.73	2.56	2.57	2.72	2.60	2.75	2.73
Tb	0.52	0.49	0.48	0.44	0.46	0.49	0.47	0.51	0.50
Dy	2.91	2.86	2.75	2.54	2.65	2.80	2.65	2.89	2.76
Ho	0.60	0.57	0.56	0.53	0.54	0.57	0.55	0.60	0.59
Er	2.06	1.94	1.93	1.80	1.87	1.94	1.86	1.99	1.99
Tm	0.37	0.36	0.36	0.33	0.33	0.37	0.34	0.37	0.34
Yb	2.62	2.45	2.47	2.35	2.34	2.54	2.36	2.57	2.42
Lu	0.43	0.40	0.41	0.38	0.38	0.40	0.39	0.43	0.40
∑REE	86.18	82.14	83.76	83.37	77.91	80.35	78.99	82.74	81.37
Cu	25.44	15.56	21.6	38.27	14.04	15.34	47.74	19.03	26.82
Zn	71.29	48.13	61.52	52.77	38.51	45.63	56.25	64.43	44.84
Ga	11.79	11.33	11.4	11.77	10.74	11.05	11	11	11.31

Table 2 *Contd...*

	SM-1-2 /1	SM-1-2 /2	SM-1-2/3	SM-1-2/4	SM-1-2/5	SM-1-2 /6	SM-1-2/7	SM-1-2/8	SM-1-2/ 9
(La/Yb) _{CN}	4.47	4.60	4.69	4.99	4.62	4.35	4.65	4.43	4.60
(La/Sm) _{CN}	3.22	3.21	3.32	3.50	3.28	3.28	3.28	3.25	3.18
(Gd/Yb) _{CN}	0.90	0.92	0.91	0.90	0.91	0.89	0.91	0.88	0.93
Eu/Eu*	0.83	0.81	0.86	0.93	0.83	0.81	0.82	0.80	0.84
Ce/Ce*	0.18	0.18	0.18	0.19	0.19	0.18	0.19	0.18	0.18
Zr/Nb	31.80	35.49	34.20	29.03	35.80	36.33	37.59	33.54	35.25
La/Nb	6.38	6.30	6.65	5.80	6.69	6.53	6.65	6.37	6.41
Nb/Ta	5.62	8.07	7.61	7.71	6.02	112.10	7.68	7.94	4.71
Zr/Sm	24.89	28.03	26.45	27.14	27.23	28.23	28.68	26.50	27.12
Th/Ce	0.20	0.20	0.20	0.20	0.20	0.20	0.20	0.20	0.19
Zr/Hf	32.56	37.15	33.81	33.94	35.66	36.65	37.03	33.36	37.06
Zr/Y	3.67	4.15	3.95	4.16	4.05	3.98	4.27	3.87	4.02
Ba/Yb	136.70	139.30	143.48	168.70	136.83	128.80	142.15	131.74	145.37
Nb/Zr	0.03	0.03	0.03	0.03	0.03	0.03	0.03	0.03	0.03
Ba/Nb	139.96	136.95	145.96	140.76	142.18	138.70	145.79	135.75	145.31
Y+Nb	24.68	23.74	23.44	22.43	22.16	23.84	22.56	24.11	23.66
Ba/La	21.93	21.74	21.96	24.26	21.26	21.24	21.91	21.32	22.66
Ce/Nb	13.27	12.92	13.64	11.95	13.52	13.22	13.42	12.93	13.11
Th/Nb	2.60	2.52	2.69	2.39	2.66	2.58	2.69	2.60	2.49
Nb/La	0.16	0.16	0.15	0.17	0.15	0.15	0.15	0.16	0.16
Th/Ta	14.62	20.34	20.49	18.45	15.99	289.19	20.67	20.66	11.73
Nb/Y	0.12	0.12	0.12	0.14	0.11	0.11	0.11	0.12	0.11
Nb/Th	0.38	0.40	0.37	0.42	0.38	0.39	0.37	0.38	0.40
La/Sm	5.00	4.98	5.14	5.43	5.09	5.07	5.08	5.03	4.93
Nd/Hf	6.39	6.42	6.29	6.34	6.38	6.40	6.21	6.07	6.57

Normalization values are from Sun and McDonough, 1989

Table 2 Contd...

<i>wt. %</i>	SV-1-08/1	SV-1-08/2	SV-1-08/3	SV-1-08/4	SV-1-08/5	SV-1-08/6	SV-1-08/7	SV-1-08/8	SV-1-08/9
SiO ₂	76.67	76.18	77.09	75.01	77.25	75.23	77.58	76.96	77.11
TiO ₂	0.18	0.17	0.17	0.16	0.16	0.16	0.17	0.17	0.18
Al ₂ O ₃	13.38	13.17	13.36	12.87	13.30	12.91	13.40	13.35	13.48
FeO	2.09	1.84	1.69	1.53	1.79	1.54	1.63	1.75	1.87
MnO	0.12	0.12	0.12	0.12	0.12	0.12	0.17	0.12	0.12
MgO	0.55	0.54	0.44	0.54	0.41	0.52	0.39	0.44	0.45
CaO	1.95	2.02	1.98	1.79	1.89	1.82	1.96	2.08	2.11
Na ₂ O	4.66	5.10	4.97	5.96	4.72	5.84	4.71	4.84	4.61
K ₂ O	1.10	1.08	1.06	1.06	1.07	1.07	1.07	1.09	1.08
P ₂ O ₅	0.04	0.04	0.04	0.04	0.04	0.04	0.04	0.04	0.04
Total	100.73	100.25	100.92	99.05	100.76	99.25	101.10	100.82	101.04
Na ₂ O+K ₂ O	5.76	6.18	6.03	7.01	5.79	6.91	5.78	5.92	5.70
<i>ppm</i>									
Cr	13.15	11.20	16.02	8.23	7.45	13.30	10.41	9.45	7.71
Co	3.33	3.51	2.85	2.28	2.65	2.42	3.24	2.81	2.95
Ni	7.04	4.75	4.64	3.03	3.01	4.16	10.14	3.53	3.47
Rb	25	24	24	21	23	22	23	24	26
Sr	130	137	137	128	132	133	130	140	142
Cs	1.14	1.06	2.23	0.84	0.95	0.87	0.98	1.03	1.88
Ba	247	253	291	227	251	238	243	260	272
Sc	4.68	4.46	4.65	4.12	4.40	4.21	4.33	4.52	4.65
V	24.32	23.09	20.28	13.11	20.66	23.78	17.60	15.48	16.59
Ta	0.39	0.37	0.29	0.35	0.37	-	0.39	0.46	1.64
Nb	2.93	2.84	2.67	2.71	2.83	2.73	2.81	2.86	2.86
Zr	134.50	135.90	148.90	133.40	138.90	135.10	138.30	140.60	142.90
Hf	3.14	3.28	3.54	3.23	3.31	3.25	3.36	3.32	3.39
Th	4.18	4.09	4.06	3.81	4.03	3.88	4.06	4.24	4.28
U	0.93	0.96	0.95	0.86	0.92	0.90	0.91	0.95	0.97
Y	25.81	26.10	26.63	25.39	26.72	25.70	26.76	26.67	26.79
La	13.01	13.08	12.98	12.27	12.99	12.47	13.05	13.21	13.58
Ce	27.94	28.23	27.98	26.76	28.16	27.16	28.27	28.75	29.36
Pr	3.19	3.22	3.20	3.05	3.24	3.14	3.24	3.30	3.35
Nd	14.29	14.41	14.60	13.89	14.55	14.08	14.49	14.93	15.02
Sm	3.45	3.45	3.48	3.29	3.59	3.48	3.57	3.61	3.64
Eu	0.85	0.85	0.87	0.80	0.85	0.80	0.86	0.87	0.88
Gd	3.17	3.12	3.25	3.05	3.24	3.16	3.28	3.31	3.29
Tb	0.58	0.61	0.61	0.57	0.60	0.60	0.61	0.61	0.62
Dy	3.39	3.45	3.47	3.38	3.57	3.41	3.52	3.56	3.62
Ho	0.71	0.70	0.73	0.70	0.73	0.71	0.73	0.75	0.71
Er	2.37	2.45	2.44	2.33	2.44	2.34	2.43	2.49	2.46
Tm	0.42	0.43	0.44	0.41	0.44	0.43	0.44	0.45	0.44
Yb	2.90	3.01	3.02	2.89	3.00	2.94	3.05	3.05	3.07
Lu	0.48	0.48	0.49	0.47	0.50	0.48	0.51	0.52	0.52
∑REE	76.74	77.49	77.56	73.86	77.90	75.20	78.04	79.41	80.54
Cu	14.39	12.87	14.64	15.52	13.43	13.5	13.31	15.98	14.34
Zn	73.15	69.16	63.3	55.35	60.64	54.16	57.48	78.43	67.58
Ga	11.1	11.25	12.95	10.09	10.96	10.36	11.3	11.16	12.06

Table 2 Contd...

	SV-1- 08/1	SV-1- 08/2	SV-1- 08/3	SV-1- 08/4	SV-1- 08/5	SV-1- 08/6	SV-1- 08/7	SV-1- 08/8	SV-1- 08/9
(La/Yb) _{CN}	3.22	3.11	3.08	3.04	3.11	3.04	3.07	3.11	3.17
(La/Sm) _{CN}	2.44	2.45	2.41	2.41	2.33	2.32	2.36	2.36	2.41
(Gd/Yb) _{CN}	0.91	0.86	0.89	0.87	0.89	0.89	0.89	0.90	0.89
Eu/Eu*	0.79	0.79	0.79	0.77	0.77	0.74	0.77	0.77	0.78
Ce/Ce*	0.18	0.18	0.18	0.19	0.18	0.18	0.18	0.18	0.18
Zr/Nb	45.90	47.87	55.79	49.32	49.05	49.58	49.18	49.23	50.04
La/Nb	4.44	4.61	4.86	4.54	4.59	4.58	4.64	4.63	4.75
Nb/Ta	7.57	7.69	9.30	7.73	7.76	-	7.25	6.22	1.75
Zr/Sm	39.03	39.36	42.78	40.55	38.67	38.88	38.78	38.95	39.30
Th/Ce	0.15	0.14	0.15	0.14	0.14	0.14	0.14	0.15	0.15
Zr/Hf	42.85	41.47	42.04	41.30	41.98	41.53	41.12	42.32	42.14
Zr/Y	5.21	5.21	5.59	5.25	5.20	5.26	5.17	5.27	5.33
Ba/Yb	85.15	83.88	96.26	78.46	83.66	81.01	79.70	85.15	88.60
Nb/Zr	0.02	0.02	0.02	0.02	0.02	0.02	0.02	0.02	0.02
Ba/Nb	84.16	89.05	108.99	83.88	88.59	87.38	86.42	90.97	95.24
Y+Nb	28.74	28.94	29.30	28.10	29.55	28.43	29.57	29.53	29.65
Ba/La	18.95	19.33	22.41	18.49	19.31	19.09	18.62	19.67	20.03
Ce/Nb	9.54	9.94	10.48	9.89	9.94	9.97	10.05	10.07	10.28
Th/Nb	1.43	1.44	1.52	1.41	1.42	1.42	1.44	1.48	1.50
Nb/La	0.23	0.22	0.21	0.22	0.22	0.22	0.22	0.22	0.21
Th/Ta	10.80	11.09	14.14	10.90	11.04	-	10.47	9.23	2.61
Nb/Y	0.11	0.11	0.10	0.11	0.11	0.11	0.11	0.11	0.11
Nb/Th	0.70	0.69	0.66	0.71	0.70	0.70	0.69	0.67	0.67
La/Sm	3.78	3.79	3.73	3.73	3.62	3.59	3.66	3.66	3.73
Nd/Hf	4.55	4.40	4.12	4.30	4.40	4.33	4.31	4.49	4.43

Normalization values are from Sun and McDonough,
1989